Supporting Information

Intramolecular chalcogen bonding to tune the molecular conformation of helical building blocks for a supramolecular helix

Peimin Weng,[a] Xiaosheng Yan,*[a,b] Jinlian Cao,[a] Zhao Li,[a] and Yun-Bao Jiang*[a]

[a]*Department of Chemistry, College of Chemistry and Chemical Engineering, The MOE Key Laboratory of Spectrochemical Analysis and Instrumentation, and Collaborative Innovation Center of Chemistry for Energy Materials (iChEM), Xiamen University, Xiamen 361005, China.*

[b]*School of Pharmaceutical Sciences, Xiamen University, Xiamen 361102, China.*

*Corresponding Authors: Xiaosheng Yan: xshyan@xmu.edu.cn; Yun-Bao Jiang: ybjiang@xmu.edu.cn

Table of Contents

1. Materials

Phenyl isothiocyanate, 4-fluorophenyl isothiocyanate, 4-chlorophenyl isothiocyanate, 4-bromophenyl isothiocyanate, 4-iodophenyl isothiocyanate, 2,5-thiophene dicarboxylic acid, 2,5-furan dicarboxylic acid, and acetonitrile for spectroscopy were purchased from Energy Chemical. L/D-alanine, were obtained from GL Biochem (shanghai) Ltd. Acetonitrile-D_3 and dimethyl sulfoxide-D_6 were purchased from Sigma Aldrich. All other starting materials were obtained from Sinopharm Chemical Reagent Ltd.

2. General methods

Absorption spectra were recorded on a Thermo Scientific Evolution 300 UV/Vis spectrophotometer. CD spectra were recorded with a JASCO J-1500 spectrometer. ^{1}H NMR, ^{13}C NMR and 2D NMR spectra were obtained on Bruker AV500 MHz, AV600 MHz or AV850 MHz spectrometer in acetonitrile-D_3 (CD_3CN), dimethyl sulfoxide-D_6 (DMSO-d_6) or mixed solvents. High-resolution mass spectra (HR-MS) were obtained on a Bruker En Apex ultra 7.0 FT-MS. SEM experiments were conducted by using a Hitachi S-4800 scanning electron microscope. AFM experiments were conducted by using an Asylum Research Cypher S equipment. DLS were collected with a Malvern Zetasizer Nano-ZS90. DFT calculations were carried out using Gaussian 16.

X-ray crystallography data of compound L,L-**TAI** was collected on an Oxford Gemini S Ultra system (Cu-Kα), D,D-**TAI** and L,L-**TACl** were collected on an Agilent SuperNova Dual system (Cu-Kα). Absorption corrections were applied by using the program CrysAlis (multi-scan). The structures were solved by direct methods using OLEX2 program package, and non-hydrogen atoms were refined anisotropically unless otherwise stated. For L,L-**TAI** and D,D-**TAI** crystals, SQUEEZE tool of PLATON was applied,[1] through which the disordered solvent molecules, *i.e.* one DMSO and three H_2O molecules in L,L-**TAI** crystal, two DMSO molecules in D,D-**TAI** crystal, were removed. For L,L-**TACl** crystal, as it was not possible to see clear electron-density peaks in difference maps which would correspond with acceptable locations for the H atoms bonded to water oxygen atom O13, the refinements were completed with no allowance for these water H atoms in the models.

3. Syntheses and characterizations

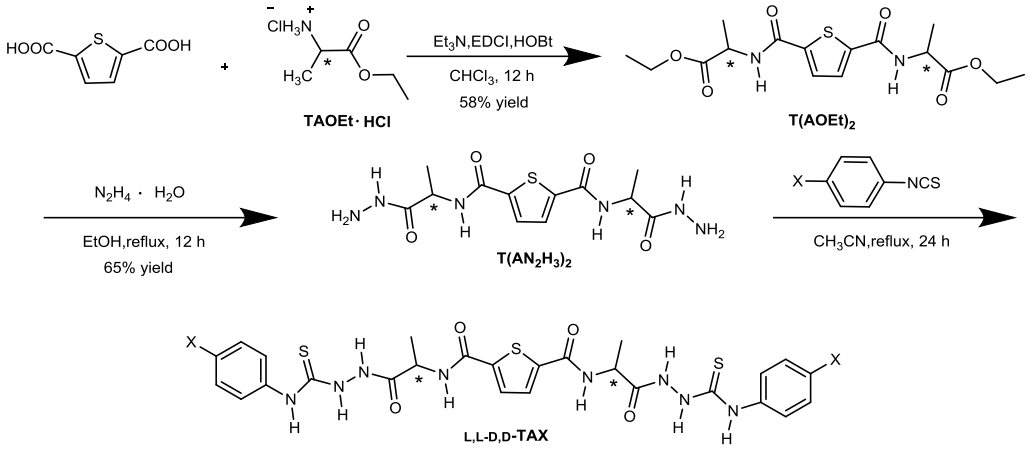

Scheme S1. Syntheses of L,L-/D,D-**TAX** (**X = H, F, Cl, Br, I**).

T(AOEt)$_2$: 1.72 g (10.0 mmol) 2,5-thiophene dicarboxylic acid was added to 30 mL $CHCl_3$, and 4 mL Et_3N was added in the ice bath dropwise to make the solution clear and transparent. Then 4.22 g (22.0 mmol) EDCI and 2.97 g (22.0 mmol) HOBT were added and stirred in the ice bath for 30 min. L-or D-**AOEt·HCl** (3.00 g, 20.0 mmol) was added to the above solution. The reaction mixture was stirred at room temperature for 12 h. The solvent was removed by evaporated *in vacuo*, 20 mL ethyl acetate and 20 mL pure water were added in turn, and the organic phase was washed with dilute $NH_3{\cdot}H_2O$ (0.1 M), dilute HCl (0.1 M) and saturated NaCl solution for several times in turn, and was dried by anhydrous $MgSO_4$. The solvent was removed by evaporated *in vacuo* to afford a white solid **T(AOEt)$_2$** (2.15 g, 58% yield).

T(AN$_2$H$_3$)$_2$: Excess aqueous hydrazine (85%, 4.0 mL) was added to **T(AOEt)$_2$** in EtOH (50 mL) and the mixture was refluxed for 12 hours. The solvent was removed by filtration, and the crude product was washed with EtOH and Et_2O several times to afford white solid product **T(AN$_2$H$_3$)$_2$** (1.29 g, 65% yield).

TAX: **T(AN$_2$H$_3$)$_2$** (0.034 g, 0.1 mmol) was added to excess (0.25 mmol) phenyl isothiocyanate with or without halogen substituent in 50 mL CH_3CN and then refluxed for 24 h. The solvent was removed by filtration, and the crude product was washed with hot CH_3CN and Et_2O for several times to afford pure white solid product **TAX** (60% yield averagely).

L,L-**TAI**

(N^2,N^5-bis((*S*)-1-(2-((4-iodophenyl)carbamothioyl)hydrazineyl)-1-oxopropan-2-yl)thiophene-2,5-dicarboxamide): ^{1}H NMR (600 MHz, DMSO-d_6) δ (ppm) 10.45 (s, 2H), 9.75 (s, 2H), 9.23 (s, 2H), 9.12 (s, 2H), 7.92 (s, 2H), 7.69 (s, 4H), 7.31 (s, 4H), 7.14 (t, J = 6.7 Hz, 2H), 4.34 (s, 2H), 1.41 (d,

J = 5.9 Hz, 6H); ^{13}C NMR (151 MHz, DMSO-d_6) δ (ppm) 179.99, 171.69, 161.83, 142.48, 138.90, 136.73, 129.66, 125.94, 89.28, 49.03, 16.47; HRMS (ESI): calcd for $[C_{26}H_{26}I_2N_8O_4S_3Na]^+$: 886.9226, found: 886.9198.

D,D-**TAI**

(N^2,N^5-bis((*R*)-1-(2-((4-iodophenyl)carbamothioyl)hydrazineyl)-1-oxopropan-2-yl)thiophene-2,5-dicarboxamide): ^{1}H NMR (600 MHz, DMSO-d_6) δ (ppm) 10.45 (s, 2H), 9.75 (s, 2H), 9.23 (s, 2H), 9.12 (s, 2H), 7.92 (s, 2H), 7.69 (s, 4H), 7.31 (s, 4H), 7.14 (t, *J* = 6.7 Hz, 2H), 4.34 (s, 2H), 1.41 (d, *J* = 5.9 Hz, 6H); ^{13}C NMR (151 MHz, DMSO-d_6) δ (ppm) 180.00, 171.68, 161.81, 142.41, 138.90, 136.74, 129.60, 125.92, 89.21, 49.10, 16.47; HRMS (ESI): calcd for $[C_{26}H_{26}I_2N_8O_4S_3Na]^+$: 886.9226, found: 886.9218.

L,L-**TAH**

(N^2,N^5-bis((*S*)-1-oxo-1-(2-(phenylcarbamothioyl)hydrazineyl)propan-2-yl)thiophene-2,5-dicarbox amide): ^{1}H NMR (600 MHz, DMSO-d_6) δ (ppm) 10.45 (s, 2H), 9.75 (s, 2H), 9.23 (s, 2H), 9.12 (s, 2H), 7.92 (s, 2H), 7.69 (s, 4H), 7.31 (s, 4H), 7.14 (t, *J* = 6.7 Hz, 2H), 4.34 (s, 2H), 1.41 (d, *J* = 5.9 Hz, 6H); ^{13}C NMR (151 MHz, DMSO-d_6) δ (ppm) 180.09, 171.64, 161.76, 142.57, 138.98, 129.47, 128.06, 124.79, 123.96, 49.05, 16.53; HRMS (ESI): calcd for $[C_{26}H_{28}N_8O_4S_3Na]^+$: 635.1293, found: 635.1278.

D,D-**TAH**

(N^2,N^5-bis((*R*)-1-oxo-1-(2-(phenylcarbamothioyl)hydrazineyl)propan-2-yl)thiophene-2,5-dicarbox amide): ^{1}H NMR (600 MHz, DMSO-d_6) δ (ppm) 10.45 (s, 2H), 9.75 (s, 2H), 9.23 (s, 2H), 9.12 (s, 2H), 7.92 (s, 2H), 7.69 (s, 4H), 7.31 (s, 4H), 7.14 (t, *J* = 6.7 Hz, 2H), 4.34 (s, 2H), 1.41 (d, *J* = 5.9 Hz, 6H); ^{13}C NMR (151 MHz, DMSO-d_6) δ (ppm) 180.06, 171.62, 161.78, 142.64, 138.98, 129.49, 128.07, 124.80, 123.94, 49.06, 16.53; HRMS (ESI): calcd for $[C_{26}H_{28}N_8O_4S_3Na]^+$: 635.1293, found: 635.1280.

L,L-**TAF**

(N^2,N^5-bis((*S*)-1-(2-((4-fluorophenyl)carbamothioyl)hydrazineyl)-1-oxopropan-2-yl)thiophene-2,5-dicarboxamide): ^{1}H NMR (600 MHz, DMSO-d_6) δ (ppm) 10.41 (s, 2H), 9.77 (s, 2H), 9.27 (s, 2H), 9.08 (s, 2H), 7.90 (s, 2H), 7.61 (s, 4H), 7.12 (s, 4H), 4.35 (s, 2H), 1.40 (s, 6H); ^{13}C NMR (151 MHz, DMSO-d_6) δ (ppm) 180.47, 171.60, 161.72, 160.01, 158.41, 135.29, 129.52, 126.31, 114.78, 114.64, 49.02, 16.62; HRMS (ESI): calcd for $[C_{26}H_{26}F_2N_8O_4S_3Na]^+$: 671.1105, found: 671.1088.

D,D-**TAF**

(N^2,N^5-bis((*R*)-1-(2-((4-fluorophenyl)carbamothioyl)hydrazineyl)-1-oxopropan-2-yl)thiophene-2,5

-dicarboxamide): ^{1}H NMR (600 MHz, DMSO-d_6) δ (ppm) 10.45 (s, 2H), 9.75 (s, 2H), 9.23 (s, 2H), 9.12 (s, 2H), 7.92 (s, 2H), 7.69 (s, 4H), 7.31 (s, 4H), 7.14 (t, J = 6.7 Hz, 2H), 4.34 (s, 2H), 1.41 (d, J = 5.9 Hz, 6H); ^{13}C NMR (151 MHz, DMSO-d_6) δ (ppm) 180.55, 171.60, 161.72, 160.04, 158.40, 135.30, 129.50, 126.30, 114.79, 114.63, 48.94, 16.60; HRMS (ESI): calcd for $[C_{26}H_{26}F_2N_8O_4S_3Na]^+$: 671.1105, found: 671.1091.

L,L-**TACl**

(N^2,N^5-bis((*S*)-1-(2-((4-chlorophenyl)carbamothioyl)hydrazineyl)-1-oxopropan-2-yl)thiophene-2,5-dicarboxamide): ^{1}H NMR (600 MHz, DMSO-d_6) δ (ppm) 10.45 (s, 2H), 9.75 (s, 2H), 9.23 (s, 2H), 9.12 (s, 2H), 7.92 (s, 2H), 7.69 (s, 4H), 7.31 (s, 4H), 7.14 (t, J = 6.7 Hz, 2H), 4.34 (s, 2H), 1.41 (d, J = 5.9 Hz, 6H); ^{13}C NMR (151 MHz, DMSO-d_6) δ (ppm) 180.15, 171.65, 161.85, 142.54, 137.98, 129.62, 128.72, 127.96, 125.54, 49.08, 16.54; HRMS (ESI): calcd for $[C_{26}H_{26}Cl_2N_8O_4S_3Na]^+$: 703.0514, found: 703.0500.

D,D-**TACl**

(N^2,N^5-bis((*R*)-1-(2-((4-chlorophenyl)carbamothioyl)hydrazineyl)-1-oxopropan-2-yl)thiophene-2,5-dicarboxamide): ^{1}H NMR (600 MHz, DMSO-d_6) δ (ppm) 10.45 (s, 2H), 9.75 (s, 2H), 9.23 (s, 2H), 9.12 (s, 2H), 7.92 (s, 2H), 7.69 (s, 4H), 7.31 (s, 4H), 7.14 (t, J = 6.7 Hz, 2H), 4.34 (s, 2H), 1.41 (d, J = 5.9 Hz, 6H); ^{13}C NMR (151 MHz, DMSO-d_6) δ (ppm) 180.13, 171.63, 161.83, 142.55, 137.98, 129.60, 128.75, 127.96, 125.56, 49.14, 16.58; HRMS (ESI): calcd for $[C_{26}H_{26}Cl_2N_8O_4S_3Na]^+$: 703.0514, found: 703.0509.

L,L-**TABr**

(N^2,N^5-bis((*S*)-1-(2-((4-bromophenyl)carbamothioyl)hydrazineyl)-1-oxopropan-2-yl)thiophene-2,5-dicarboxamide): ^{1}H NMR (600 MHz, DMSO-d_6) δ (ppm) 10.45 (s, 2H), 9.75 (s, 2H), 9.23 (s, 2H), 9.12 (s, 2H), 7.92 (s, 2H), 7.69 (s, 4H), 7.31 (s, 4H), 7.14 (t, J = 6.7 Hz, 2H), 4.34 (s, 2H), 1.41 (d, J = 5.9 Hz, 6H); ^{13}C NMR (151 MHz, DMSO-d_6) δ (ppm) 180.07, 171.67, 161.86, 142.56, 138.43, 130.90, 129.64, 125.85, 116.97, 49.07, 16.55; HRMS (ESI): calcd for $[C_{26}H_{26}Br_2N_8O_4S_3Na]^+$: 790.9504, found: 790.9486.

D,D-**TABr**

(N^2,N^5-bis((*R*)-1-(2-((4-bromophenyl)carbamothioyl)hydrazineyl)-1-oxopropan-2-yl)thiophene-2,5-dicarboxamide): ^{1}H NMR (600 MHz, DMSO-d_6) δ (ppm) 10.45 (s, 2H), 9.75 (s, 2H), 9.23 (s, 2H), 9.12 (s, 2H), 7.92 (s, 2H), 7.69 (s, 4H), 7.31 (s, 4H), 7.14 (t, J = 6.7 Hz, 2H), 4.34 (s, 2H), 1.41 (d, J = 5.9 Hz, 6H); ^{13}C NMR (151 MHz, DMSO-d_6) δ (ppm) 180.09, 171.67, 161.81, 142.52,

138.42, 130.89, 129.65, 125.85, 116.94, 49.09, 16.55; HRMS (ESI): calcd for $[C_{26}H_{26}Br_2N_8O_4S_3Na]^+$: 790.9504, found: 790.9489.

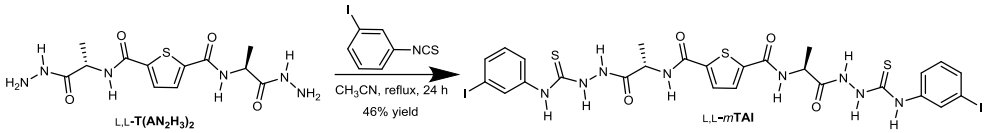

Scheme S2. Syntheses of L,L-*m***TAI**.

L,L-*m***TAI**: L,L-**T(AN$_2$H$_3$)$_2$** (0.034 g, 0.1 mmol) was added to excess 3-iodine phenyl isothiocyanate (0.065 g, 0.25 mmol) in 50 mL CH_3CN and then refluxed for 24 h. The crude product was washed with hot CH_3CN and Et_2O several times to afford pure white solid product L,L-*m***TAI**.

L,L-*m***TAI**

(N^2,N^5-bis((*S*)-1-(2-((3-iodophenyl)carbamothioyl)hydrazineyl)-1-oxopropan-2-yl)thiophene-2,5-dicarboxamide): ^{1}H NMR (600 MHz, DMSO-d_6) δ (ppm) 10.46 (s, 2H), 9.89 (s, 2H), 9.26 (s, 2H), 9.10 (s, 2H), 8.11 (s, 2H), 7.91 (s, 2H), 7.71 (s, 2H), 7.49 (d, J = 7.0 Hz, 2H), 7.08 (s, 2H), 4.33 (s, 2H), 1.40 (d, J = 5.8 Hz, 6H); ^{13}C NMR (151 MHz, DMSO-d_6) δ (ppm) 179.91, 171.51, 161.69, 142.34, 140.25, 133.19, 131.89, 129.87, 129.41, 123.21, 93.31, 48.89, 16.42. HRMS (ESI): calcd for $[C_{26}H_{26}I_2N_8O_4S_3Na]^+$: 886.9221, found:886.9205.

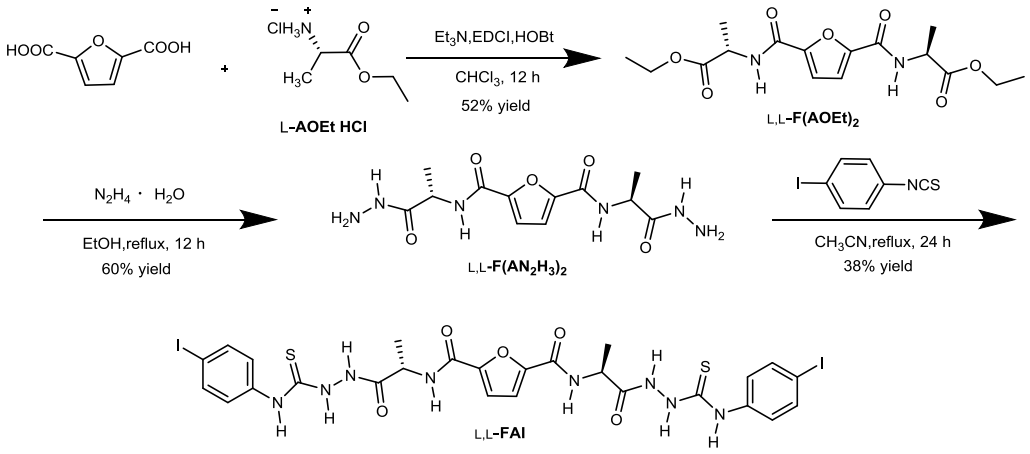

Scheme S3. Syntheses of L,L-**FAI**.

L,L-**F(AOEt)$_2$**: 1.56 g (10.0 mmol) 2,5-furan dicarboxylic acid was added to 30 mL $CHCl_3$, and 6 mL Et_3N was added in the ice bath dropwise to make the solution clear and transparent. Then 4.22 g (22.0 mmol) EDCI and 2.97 g (22.0 mmol) HOBT were added and stirred in the ice bath for 30 min. L-**AOEt·HCl** (3.00 g, 20.0 mmol) was added to the above solution. The reaction mixture was stirred at room temperature for 12 h. The solvent was removed by evaporated *in vacuo*, 20 mL

ethyl acetate and 20 mL pure water were added in turn, and the organic phase was washed with dilute $NH_3{\cdot}H_2O$ (0.1 M), dilute HCl (0.1 M) and saturated NaCl solution for several times in turn, and was dried by anhydrous $MgSO_4$. The solvent was removed by evaporated *in vacuo* to afford light yellow oily liquid L,L-**F(AOEt)$_2$** (1.84 g, 52% yield).

L,L-**F(AN$_2$H$_3$)$_2$**: Excess aqueous hydrazine (85%, 5.0 mL) was added to L,L-**F(AOEt)$_2$** in EtOH (50 mL) and the mixture was refluxed for 12 hours. The solvent was removed by evaporated *in vacuo*, and the crude product was purified by column chromatographic (CH_2Cl_2/CH_3OH = 10/1, v/v) to afford white solid product L,L-**F(AN$_2$H$_3$)$_2$** (1.02 g, 60% yield).

L,L-**FAI**: L,L-**F(AN$_2$H$_3$)$_2$** (0.065 g, 0.2 mmol) was added to excess 4-iodophenyl isothiocyanate (0.13 g, 0.5 mmol) in CH_3CN (50 mL) and then refluxed for the night. The solvent was removed by filtration, and the crude product was washed with hot CH_3CN and Et_2O several times to afford pure white solid product L,L-**FAI** (0.066 g, 38% yield).

L,L-**FAI**

(N^2,N^5-bis((*S*)-1-(2-((4-iodophenyl)carbamothioyl)hydrazineyl)-1-oxopropan-2-yl)furan-2,5-dicar boxamide): ^{1}H NMR (500 MHz, DMSO-d_6) δ (ppm) 10.40 (s, 2H), 9.82 (s, 2H), 9.31 (s, 2H), 8.85 (s, 2H), 7.68 (d, *J* = 8.2 Hz, 4H), 7.50 (s, 4H), 7.27 (s, 2H), 4.47 (s, 2H), 1.43 (d, *J* = 6.6 Hz, 6H); ^{13}C NMR (151 MHz, DMSO-d_6) δ (ppm) 180.15, 171.35, 157.85, 147.86, 139.01, 136.88, 126.36, 115.63, 89.21, 48.16, 17.04; HRMS (ESI): calcd for $[C_{26}H_{26}I_2N_8O_5S_2Na]^+$: 870.9455, found: 870.9435.

4. Experimental data

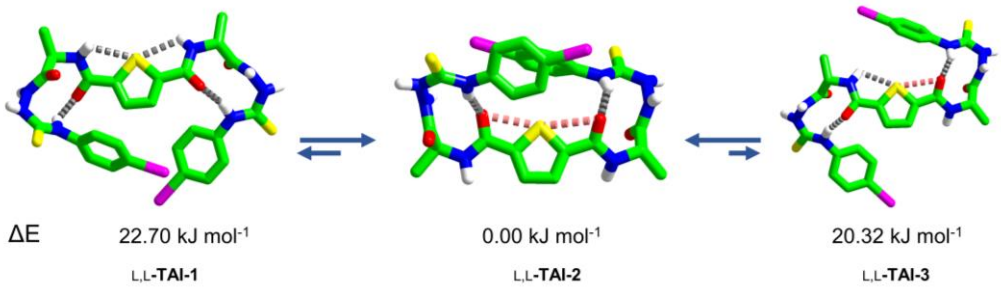

Figure S1. DFT (M062X/DEF2SVP) optimized structures of L,L-**TAI**. Dashed gray lines and pink lines highlight intramolecular hydrogen bonds and chalcogen bonds, respectively. Method: DFT M062X with the DEF2SVP basis set for C, H, O, N, S atoms, SDD for I atoms. For clarity, −CH hydrogen atoms are omitted.

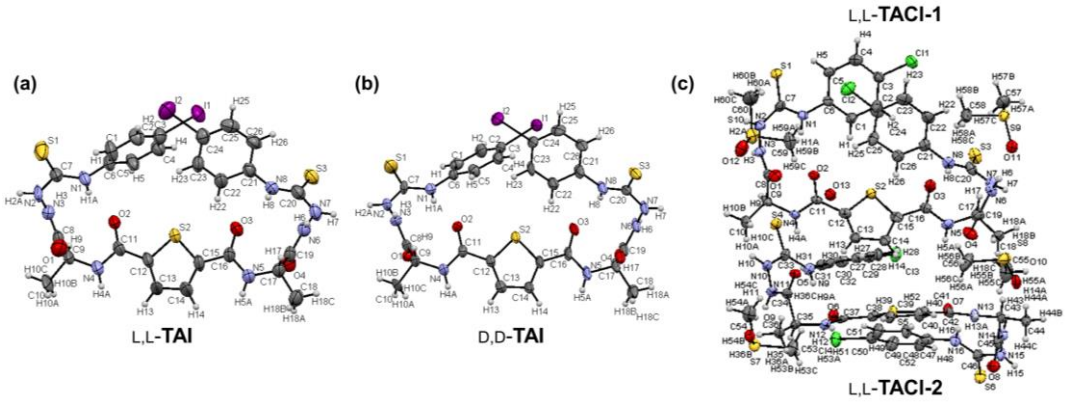

Figure S2. The labelled ORTEP plots of crystal structures of L,L-**TAI** (a), D,D-**TAI** (b) and L,L-**TACl** (c) with ellipsoids shown at the 50% probability level (arbitrary spheres for H atoms).

Table S1. Crystallographic data for L,L-/D,D-**TAI** and L,L-**TACl**

Compound reference	L,L-**TAI**	D,D-**TAI**	L,L-**TACl**
Empirical formula	$C_{26}H_{26}I_2N_8O_4S_3$	$C_{26}H_{26}I_2N_8O_4S_3$	$2(C_{26}H_{26}Cl_2N_8O_4S_3)$,$4(C_2H_6OS)$,H_2O
Formula weight	864.53	864.53	1693.78
Temperature/K	293(2)	100.00(10)	100.00(10)
Crystal system	monoclinic	monoclinic	triclinic
Space group	$P2_1$	$P2_1$	P1
a/Å	15.2990(5)	15.1996(5)	10.4905(4)
b/Å	8.9898(2)	8.9709(3)	13.1870(6)
c/Å	16.3700(6)	16.2399(4)	14.9172(7)
α/°	90	90	77.077(4)
β/°	101.785(4)	102.576(3)	88.059(3)
γ/°	90	90	80.043(3)
Volume/$Å^3$	2203.99(12)	2161.25(11)	1981.03(15)
Z	2	2	1
$\rho_{calc}g/cm^3$	1.303	1.328	1.418
μ/mm^{-1}	12.819	13.073	4.383
F(000)	848.0	848.0	880.0
Crystal size/mm^3	0.22 × 0.16 × 0.12	0.104 × 0.04 × 0.031	0.32 × 0.26 × 0.16
Radiation	CuKα (λ = 1.54184)	CuKα (λ = 1.54184)	CuKα (λ = 1.54184)
2Θ range for data collection/°	5.514 to 124.35	7.22 to 136.752	6.978 to 145.626
Index ranges	$-16 \le h \le 17$, $-9 \le k \le 10$, $-18 \le l \le 18$	$-12 \le h \le 17$, $-10 \le k \le 10$, $-19 \le l \le 17$	$-9 \le h \le 12$, $-15 \le k \le 16$, $-18 \le l \le 18$
Reflections collected	12402	8309	13179
Independent reflections	5743 [R_{int} = 0.0613, R_{sigma} = 0.0738]	5267 [R_{int} = 0.0562, R_{sigma} = 0.0678]	8821 [R_{int} = 0.0647, R_{sigma} = 0.0740]
Data/restraints/parameters	5743/1/390	5267/127/390	8821/3/940
Goodness-of-fit on F^2	1.038	1.075	1.041
Final R indexes [I>=2σ (I)]	R_1 = 0.0506, wR_2 = 0.1327	R_1 = 0.0594, wR_2 = 0.1616	R_1 = 0.0864, wR_2 = 0.2332
Final R indexes [all data]	R_1 = 0.0524, wR_2 = 0.1369	R_1 = 0.0671, wR_2 = 0.1703	R_1 = 0.0940, wR_2 = 0.2437
Largest diff. peak/hole / e $Å^{-3}$	1.00/-0.89	1.45/-1.41	1.19/-0.54
Flack parameter	0.005(8)	0.056(11)	-0.02(3)
CCDC number	2024506	2016214	2016215

Table S2. Torsions, types, bond lengths and bond angles of β-turns revealed by the X-ray crystal structures of L,L-/D,D-**TAI** and L,L-**TACl**

Compound	β-turn	φ_{i+1} / º	ψ_{i+1} / º	φ_{i+2} / º	ψ_{i+2} / º	Type	Length / Å	Angle / º
L,L-**TAI**	β1	-61.7(11)	128.2(9)	85.5(12)	7.1(14)	II	2.396(6)	148.1(5)
L,L-**TAI**	β2	-55.1(12)	127.4(10)	87.2(13)	-4.6(14)	II	2.089(7)	156.6(6)
D,D-**TAI**	β1'	66.9(17)	-129.4(13)	-84.3(18)	-9.3(20)	II'	2.378(9)	147.7(7)
D,D-**TAI**	β2'	56.3(16)	-127.5(14)	-86.8(18)	2.9(19)	II′	2.092(9)	156.5(8)
L,L-**TACl-1**	β1	-63.8(10)	124.4(9)	102.9(12)	-7.7(15)	II	2.203(8)	157.6(6)
L,L-**TACl-1**	β2	-60.6(12)	133.0(9)	91.5(13)	-9.9(16)	II	2.023(8)	156.8(6)
L,L-**TACl-2**	β1	-64.0(11)	129.0(9)	90.5(12)	-7.1(14)	II	1.976(7)	159.7(6)
L,L-**TACl-2**	β2	-58.4(12)	127.2(9)	102.3(12)	-11.5(15)	II	2.236(9)	155.5(7)

Table S3. Bond lengths and bond angles of S···O chalcogen bonds revealed by the X-ray crystal structures of L,L-/D,D-**TAI** and L,L-**TACl**

Compound	S···O ChB	Length / Å	Angle (C−S···O) / º
L,L-**TAI**	$S^3\cdots O^1$	2.977(7)	144.8(4)
L,L-**TAI**	$S^3\cdots O^2$	2.920(7)	145.0(4)
D,D-**TAI**	$S^3\cdots O^1$	2.976(10)	144.6(5)
D,D-**TAI**	$S^3\cdots O^2$	2.931(9)	144.7(4)
L,L-**TACl-1**	$S^3\cdots O^1$	2.845(8)	146.2(4)
L,L-**TACl-1**	$S^3\cdots O^2$	2.837(8)	146.7(4)
L,L-**TACl-2**	$S^3\cdots O^1$	2.820(8)	147.0(4)
L,L-**TACl-2**	$S^3\cdots O^2$	2.854(8)	146.4(4)

Table S4. Natural bond orbital[2] (NBO) analysis[a] for the intramolecular C−S ··O chalcogen bonds in monomer of L,L-**TAI** and intermolecular C−I ··S halogen bond in dimer of L,L-**TAI**.

Interaction	Donor[b]	Acceptor	$E^{(2)}$ (kJ mol^{-1})[c]
$C-S^3\cdots O^1$	$LP(2)(O^1)$	$\sigma^*(C-S^3)$	3.09
$C-S^3\cdots O^2$	$LP(2)(O^2)$		4.26
$C-I^2\cdots S^1$	$LP(1)(S^1)$	$\sigma^*(C-I^2)$	2.17
$C-I^2\cdots S^1$	$LP(2)(S^1)$		1.00

[a] Method: WB97XD DFT with the 6-31+G(d,p) basis set for C, H, O, N, S, and LANL2DZ for I atoms. POP = NBO. [b] For LP, (1) and (2) denote the first and the second lone pair electron, respectively. [c] The second-order perturbation energy.

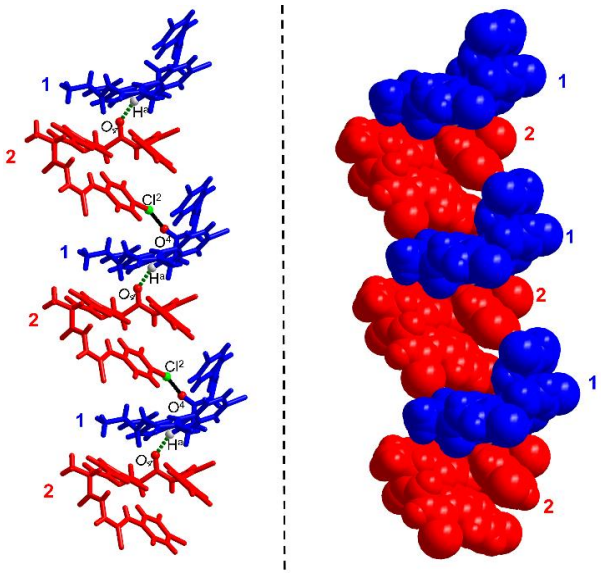

Figure S3. Crystal packing of L,L-**TACl**. Dashed green lines and black lines indicate N−H···O hydrogen bond and Cl···O halogen bond. It is seen that the **TACl** molecules form a non-helical zig-zag structure, different from the supramolecular helix of **TAI** (Fig. 3).

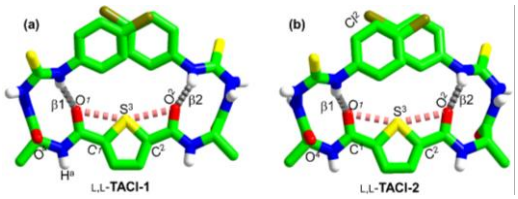

Figure S4. X-ray crystal structures of L,L-**TACl**. Dashed gray lines and pink lines highlight intramolecular hydrogen bonds and chalcogen bonds, respectively. The β-turn structures are labelled as β1 and β2, respectively. It is noted that the two intramolecular S···O=C chalcogen bonds and the two terminal β-turns, seen in L,L-**TAI**, exist too.

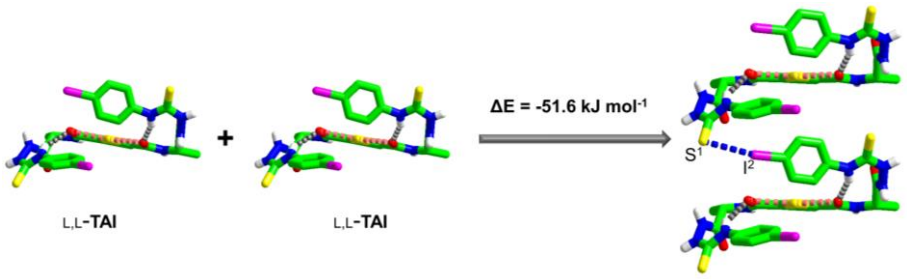

Figure S5. Structural illustration for the calculation of the overall interaction energy in the dimer of L,L-**TAI** with a C−I^2 ··S^1 halogen bond. The geometries of the two monomers and the dimer were fixed according to the X-ray crystal structures. Method: WB97XD DFT with the 6-31+G(d,p) basis set for C, H, O, N, S, and LANL2DZ for I atoms. The interaction energy = energy of the dimer − energy of two separated monomers, no counterpoise correction was applied.

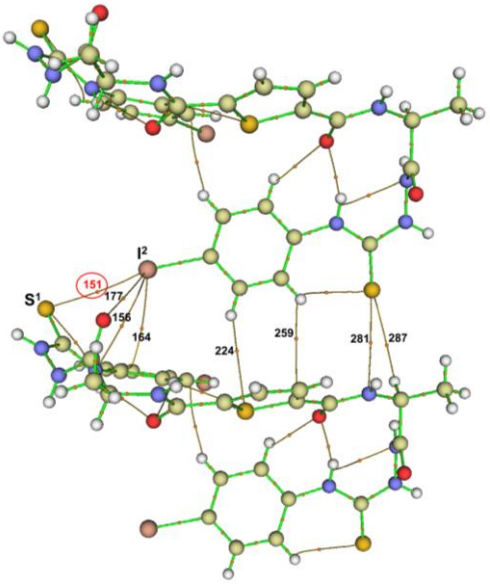

Figure S6. Topology paths in the dimer of L,L-**TAI** with labelled intermolecular critical points analyzed by Quantum Theory of Atoms In Molecules (QTAIM).[3] The presence of critical point 151 (red circle) indicates the existence of an interaction between atoms I^2 and S^1. Method: WB97XD DFT with the 6-31+G(d,p) basis set for C, H, O, N, S, and LANL2DZ for I atoms.

Table S5. Topological parameters (ρ and $\nabla^2\rho$) of the intermolecular critical point 151 (Figure S6) for C−I^2 ··S^1 halogen bond in L,L-**TAI** dimer and the calculated interaction energy (E_{nb}).[4]

Critical point	Contact	ρ	$\nabla^2\rho$	E_{nb} (kJ mol^{-1})
151	C−I^2 ··S^1	0.009	0.027	-7.61

Table S6. Topological parameters (ρ and $\nabla^2\rho$) of the intermolecular critical points (Figure S6) for van der Waals interactions in L,L-**TAI** dimer.[a]

Critical point	Contact	ρ	$\nabla^2\rho$
156	C−I···N	0.007	0.021
164	Ar−H···I	0.008	0.022
177	C−I···O	0.004	0.012
224	Ar−H···S	0.004	0.012
259	Ar−H···C	0.002	0.006
281	C−S···N	0.004	0.010
287	C−H···S	0.004	0.016

[a] The Laplacian ($\nabla^2\rho$) values are smaller than 0.024, indicating that these interactions exist as van der Waals interactions.[5]

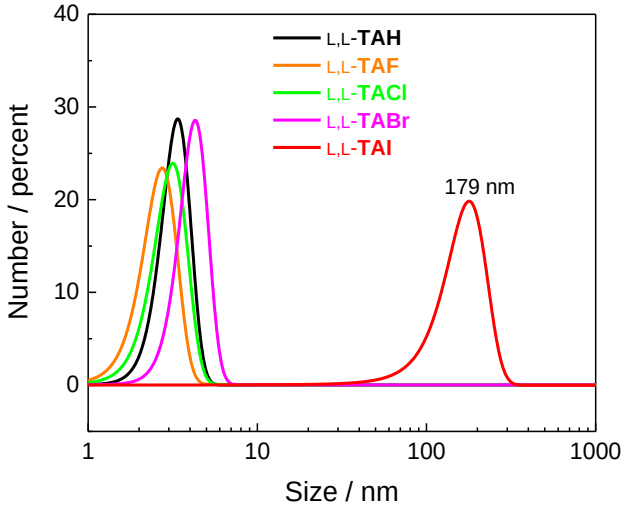

Figure S7. Hydrodynamic diameters of L,L-**TAX** (**X** = **H**, **F**, **Cl**, **Br**, **I**) in CH_3CN measured by dynamic light scattering at 25 ℃. [L,L-**TAX**] = 30 μM.

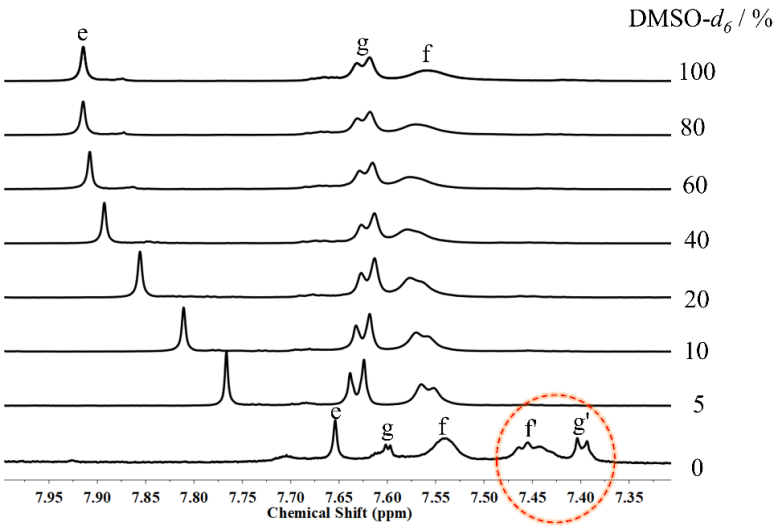

Figure S8. Partial ^{1}H NMR spectra of hydrogen atoms on benzene rings (H^e, H^f and H^g) of L,L-**TAI** in DMSO-d_6/CD_3CN mixtures of increasing volume fraction of DMSO-d_6 (850 MHz, 25 ℃). [L,L-**TAI**] = 2 mM (DMSO-d_6 = 5%-100%), [L,L-**TAI**] = 30 μM in CD_3CN. Different from those in DMSO-d_6/CD_3CN mixture in which **TAI** exists in monomeric form, ^{1}H NMR in CD_3CN shows two more aromatic hydrogen atom peaks at higher field, which are assigned to the hydrogen atoms on iodophenyl rings ($H^{f'}$ and $H^{g'}$) of the oligomers of **TAI** and confirmed by their lower diffusion coefficients (Table S7).

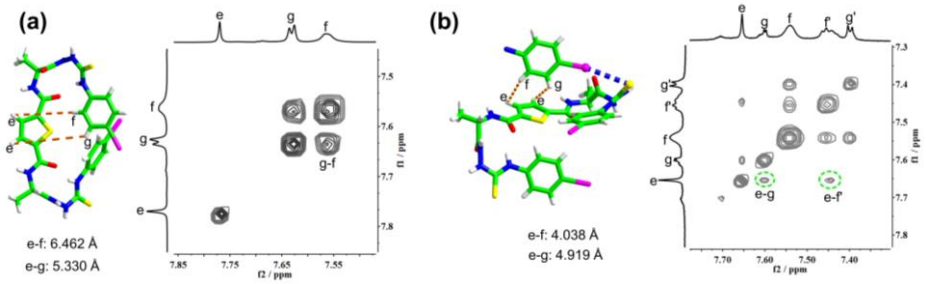

Figure S9. (a) Crystal structure of **TAI** with hydrogen atoms and distances labelled and expanded 2D NOESY spectrum of **TAI** monomer in 5:95 (v/v) DMSO-d_6/CD_3CN that shows no coupling between hydrogen atoms H^e and H^f, and H^e and H^g, due to long *intramolecular* distances of H^e-H^f (6.462 Å) and H^e-H^g (5.330 Å) seen in the crystal structure. [**TAI**] = 2 mM; 850 MHz, 25 ℃, mixing time = 600 ms. (b) Crystal structure with hydrogen atoms and distances labelled for **TAI** in dimer and expanded 2D NOESY spectrum in CD_3CN showing couplings between hydrogen atoms on phenyl rings in **TAI**. [**TAI**] = 30 μM; 850 MHz, 25 ℃, mixing time = 600 ms. NOE peaks between hydrogen atoms H^e and $H^{f'}$, and H^e and H^g are observed in CD_3CN, being thereby attributed to the *intermolecular* couplings. Indeed, from the crystal structure of **TAI**, shorter distances are measured for $H^{e/e'}$-$H^{f/f'}$ (4.038 Å) and $H^{e/e'}$-$H^{g/g'}$ (4.919 Å) between the adjacent two **TAI** molecules that are held together by the C−I···S halogen bond.

Table S7. Diffusion coefficients (D) and polymerization degrees (n) of **TAI** (30 μM) in CD_3CN.

Hydrogen atom	D (m^2/s)	n
H^e	$1.614*10^{-9}$	/
H^f	$1.516*10^{-9}$	/
$H^{f'}$	$1.139*10^{-9}$	2.48
$H^{g'}$	$1.270*10^{-9}$	1.79

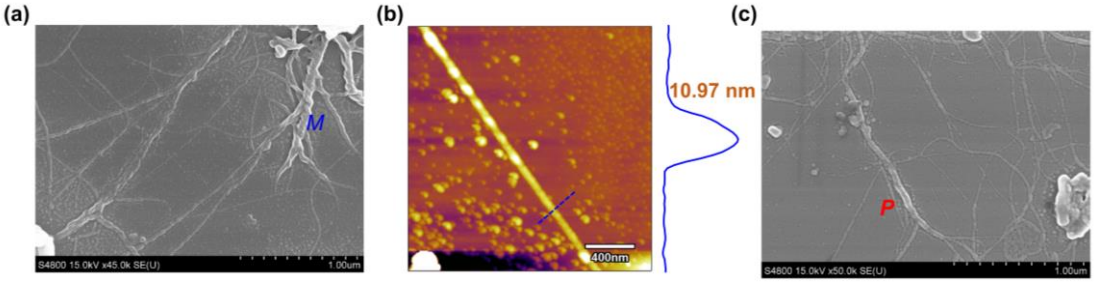

Figure S10. SEM image (a) and AFM image (b) with height profile along the blue dashed line of an air-dried sample from CH_3CN solution of L,L-**TAI** on silicon wafers, (c) SEM image of D,D-**TAI**. The particles might be dust particles that were accidentally introduced during the experiments, or that the monomeric species in the solution formed solid particles during the dryness. [L,L-**TAI**] = [D,D-**TAI**] = 30 μM.

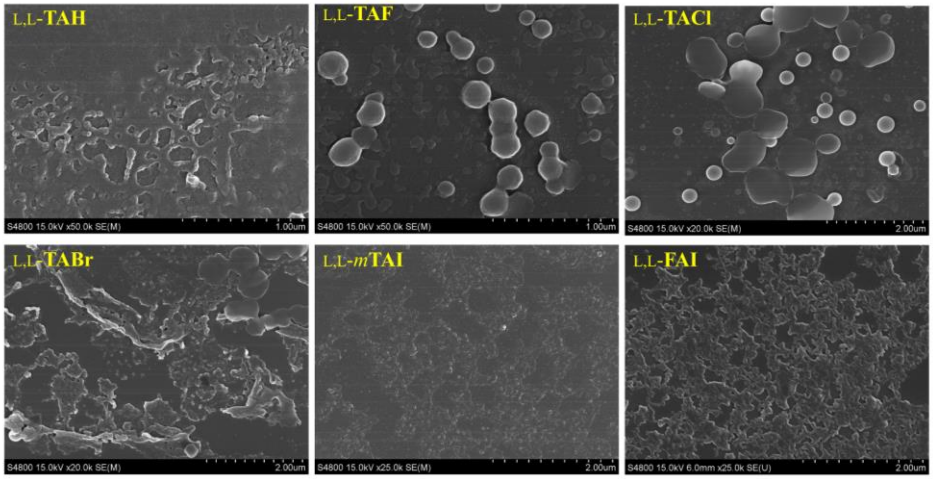

Figure S11. SEM images of air-dried samples from CH_3CN solutions of L,L-**TAX** (**X** = **H**, **F**, **Cl**, **Br**), L,L-*m***TAI** and L,L-**FAI** on platinum coated silicon wafers. [L,L-**TAX**] = [L,L-*m***TAI**] = [L,L-**FAI**] = 30 μM.

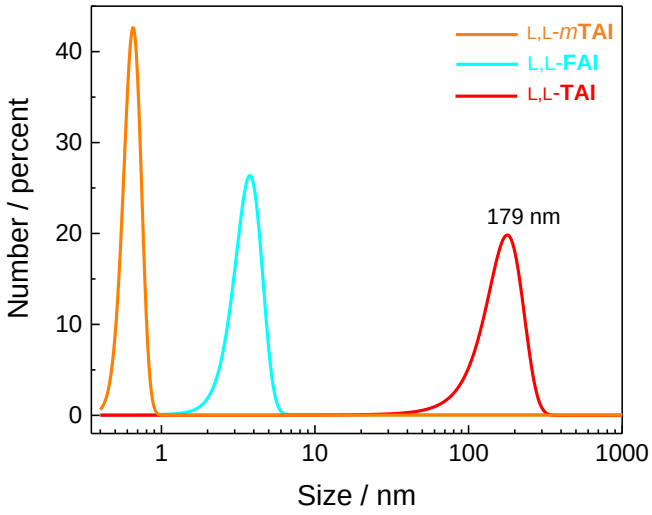

Figure S12. Hydrodynamic diameters of L,L-*m***TAI**, L,L-**FAI** and L,L-**TAI** in CH_3CN measured by dynamic light scattering. [L,L-*m***TAI**] = [L,L-**FAI**] = [L,L-**TAI**] = 30 μM.

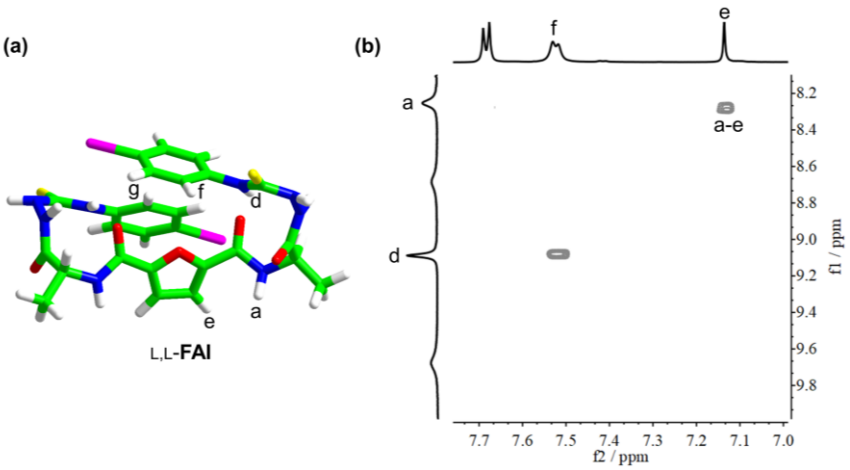

Figure S13. (a) DFT (m062x/def2svp) optimized structures of L,L-**FAI**, showing favored *cis*-conformation. Method: DFT m062x with the def2svp basis set for C, H, O, N, S atoms, sdd for I atoms. (b) Expanded 2D NOESY spectra of L,L-**FAI** in DMSO-d_6/CD_3CN (5/95, v/v) (600 MHz, 25 ℃, mixing time: 600 ms). The coupling between hydrogen atoms H^a and H^e further support the favored *cis*-conformation of L,L-**FAI**. [L,L-**FAI**] = 2 mM.

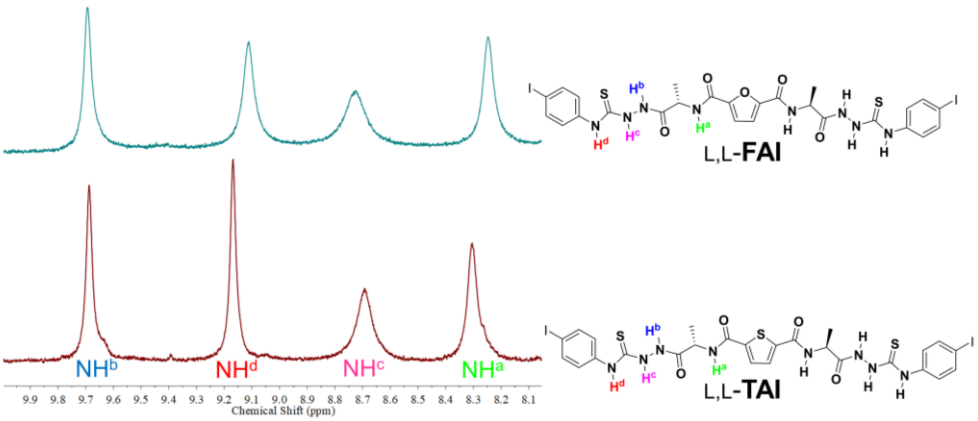

FWHM / Hz	L,L-**FAI**	L,L-**TAI**
NH^a	36.09	23.41
NH^b	22.98	15.06
NH^c	90.10	35.54
NH^d	36.09	13.52

Figure S14. Partial ^{1}H NMR spectra on -NHs of L,L-**TAI** and L,L-**FAI** in 5/95 (v/v) DMSO-d_6/CD_3CN mixtures (600 MHz) and measured values of full width at half maximum (FWHM). [L,L-**TAI**] = [L,L-**FAI**] = 2 mM.

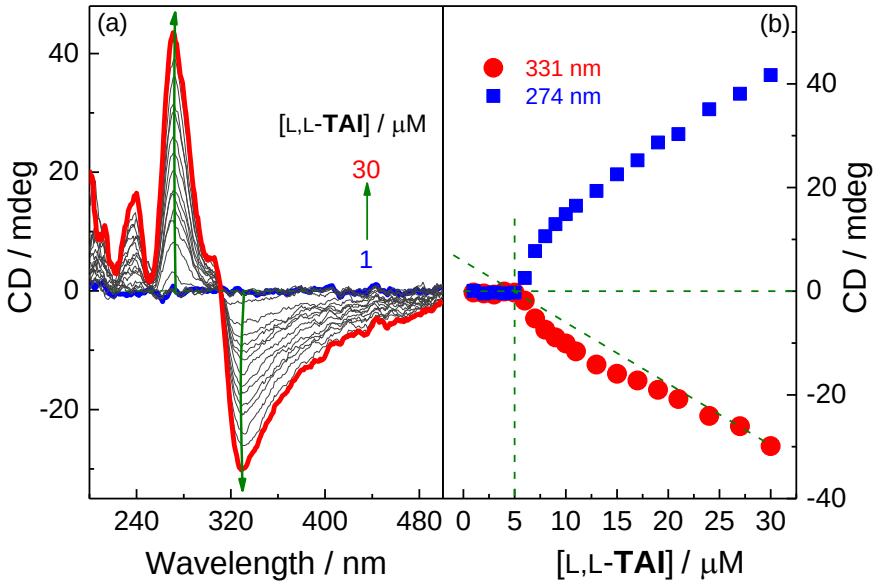

Figure S15. Concentration-dependent CD spectra of L,L-**TAI** in CH_3CN (a) and plots of CD signals at 274 nm and 331 nm versus the concentration of L,L-**TAI** (b). [L,L-**TAI**] = 1 - 30 μM.

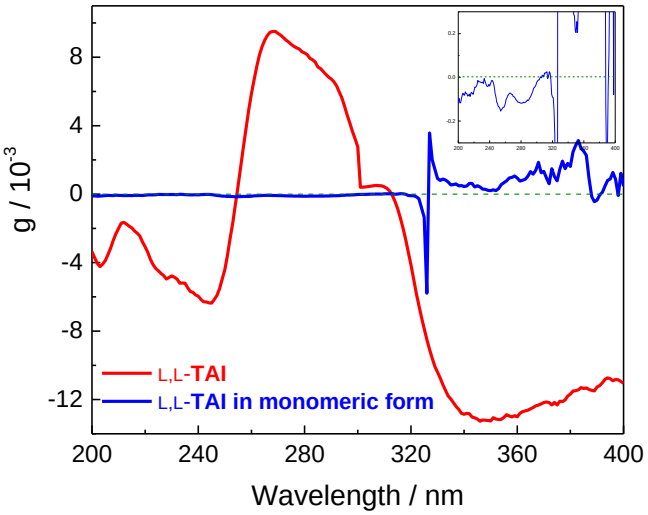

Figure S16. The anisotropy factors *g* of L,L-**TAI** in CH_3CN and in CH_3CN/H_2O (90:10, v/v) mixtures, in which L,L-**TAI** exists in a monomeric form that the water moelcules break the intermolecular halogen bonding. [L,L-**TAI**] = 30 μM.

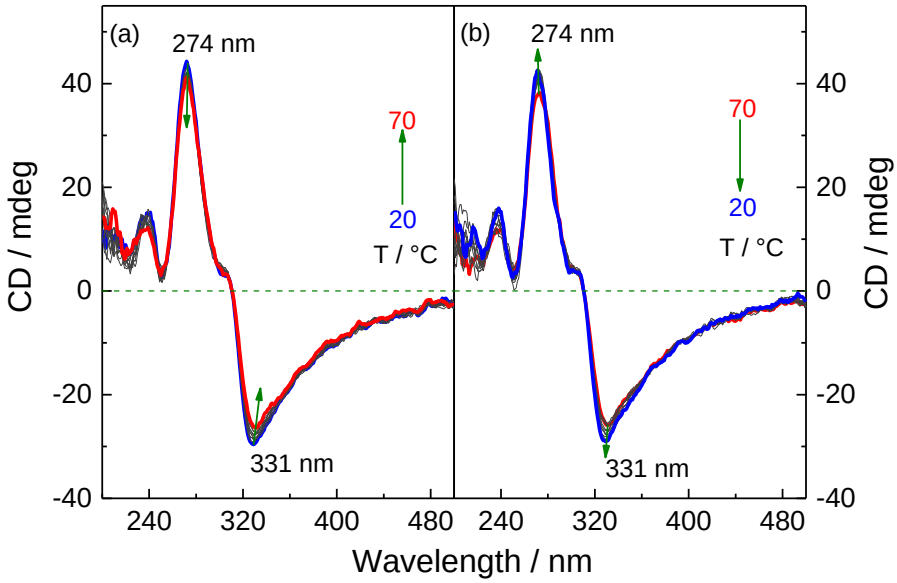

Figure S17. Temperature-dependent (20 to 70 ℃) (a) and (70 to 20 ºC) (b) CD spectra of L,L-**TAI** in CH_3CN. [L,L-**TAI**] = 30 μM.

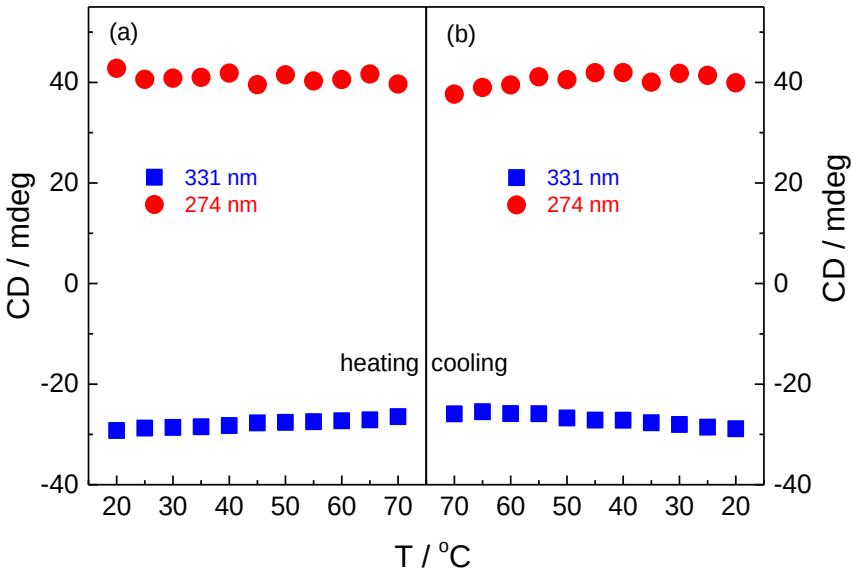

Figure S18. Plots of CD intensities at 274 and 331 nm versus solution temperature during heating (a) and followed cooling (b) processes. [L,L-**TAI**] = 30 μM.

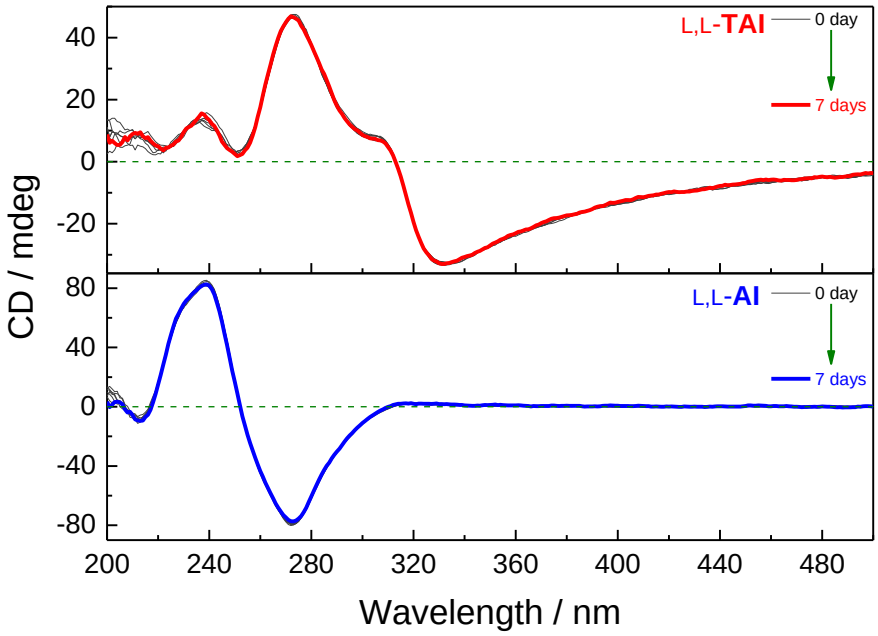

Figure S19. Time-dependent CD spectra of L,L-**AI** and L,L-**TAI** in CH_3CN solution. [L,L-**AI**] = [L,L-**TAI**] = 30 μM.

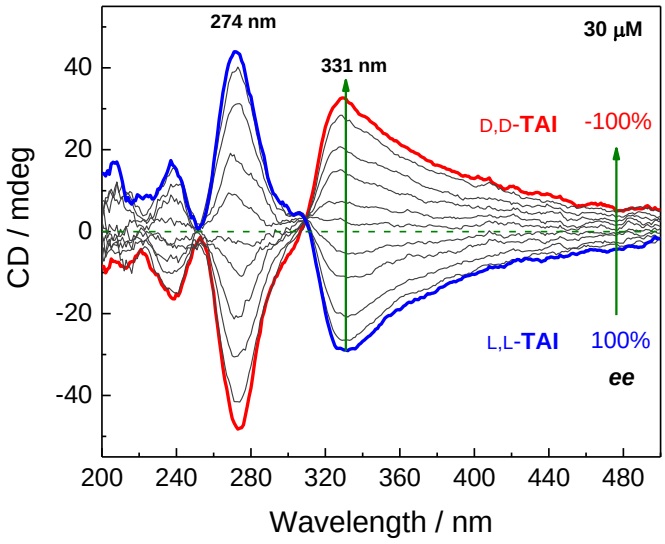

Figure S20. CD spectra of **TAI** of varying *ee* in CH_3CN at 25 ℃. [L,L-**TAI**] + [D,D-**TAI**] = 30 μM. The spectra were recorded immediately after mixing the two enantiomeric solutions.

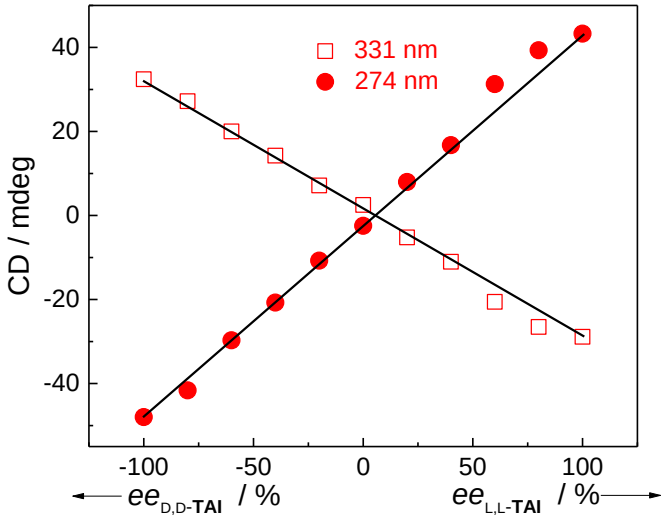

Figure S21. Plots of CD signals at 274 nm and 331 nm of **TAI** of varying *ee* in CH_3CN. [L,L-**TAI**] + [D,D-**TAI**] = 30 μM. The spectra were recorded immediately after mixing the two enantiomeric solutions.

5. ^{1}H NMR and ^{13}C NMR spectra

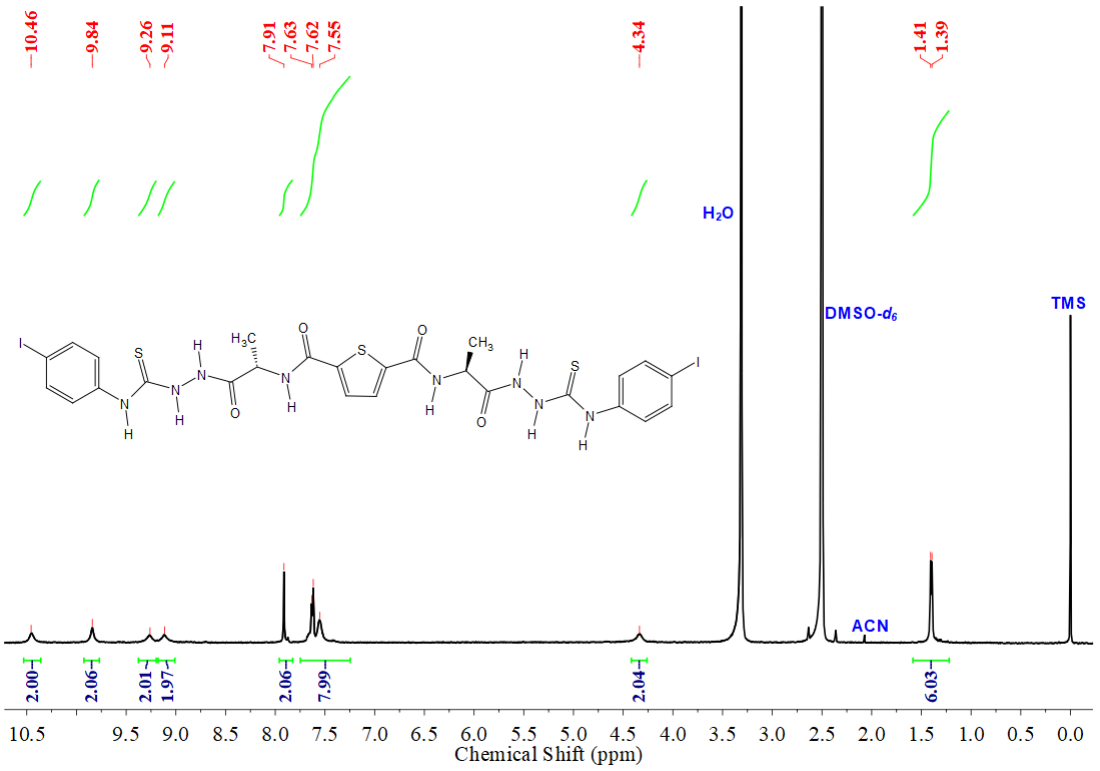

Figure S22. ^{1}H NMR (600 MHz, DMSO-d_6) spectrum of isolated product L,L-**TAI**.

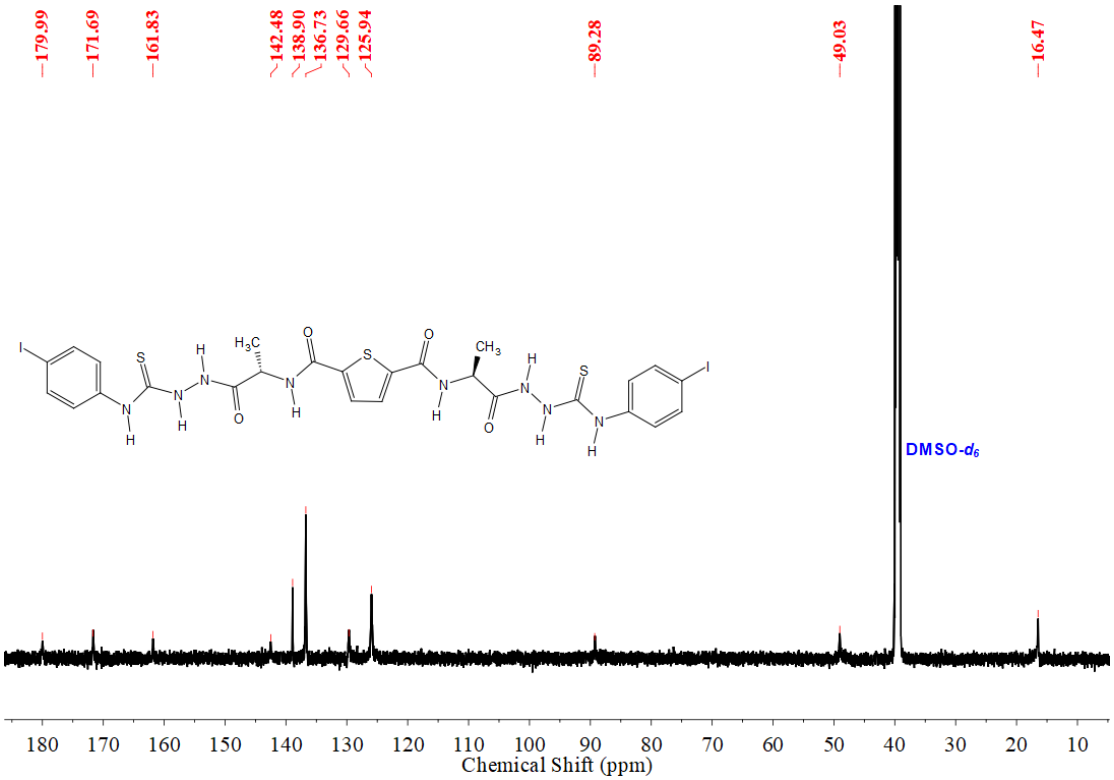

Figure S23. ^{13}C{^{1}H} NMR (151 MHz, DMSO-d_6) spectrum of isolated product L,L-**TAI**.

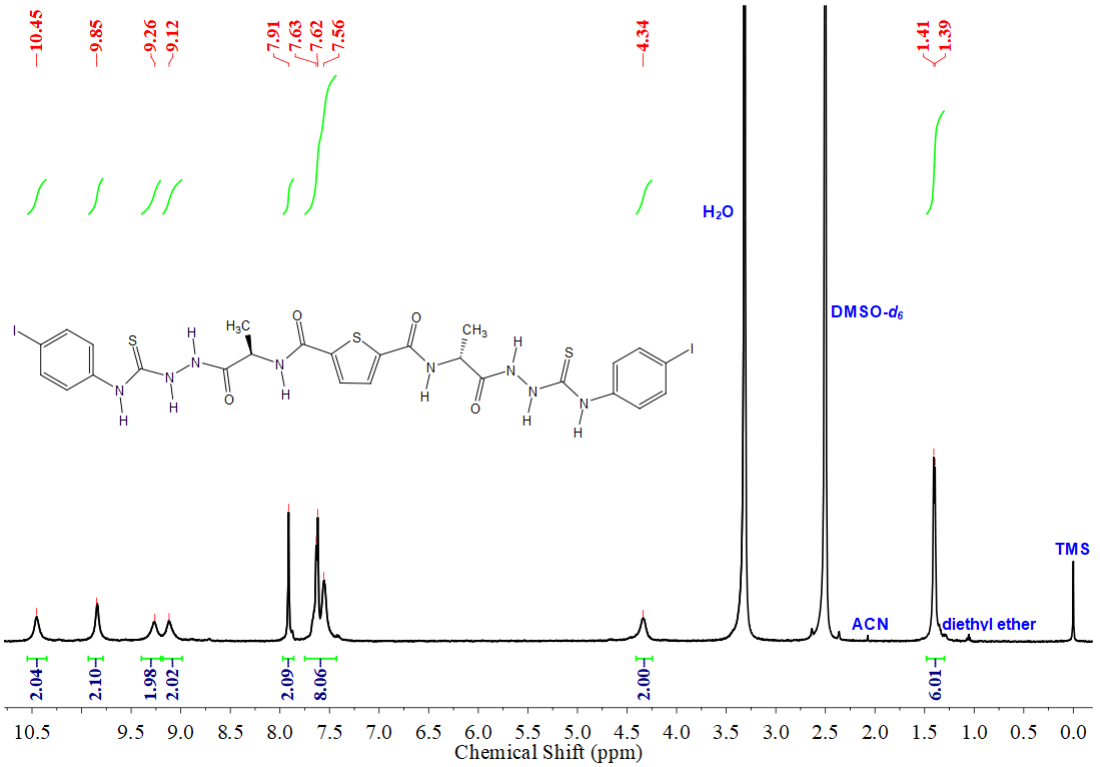

Figure S24. ^{1}H NMR (600 MHz, DMSO-d_6) spectrum of isolated product D,D-**TAI**.

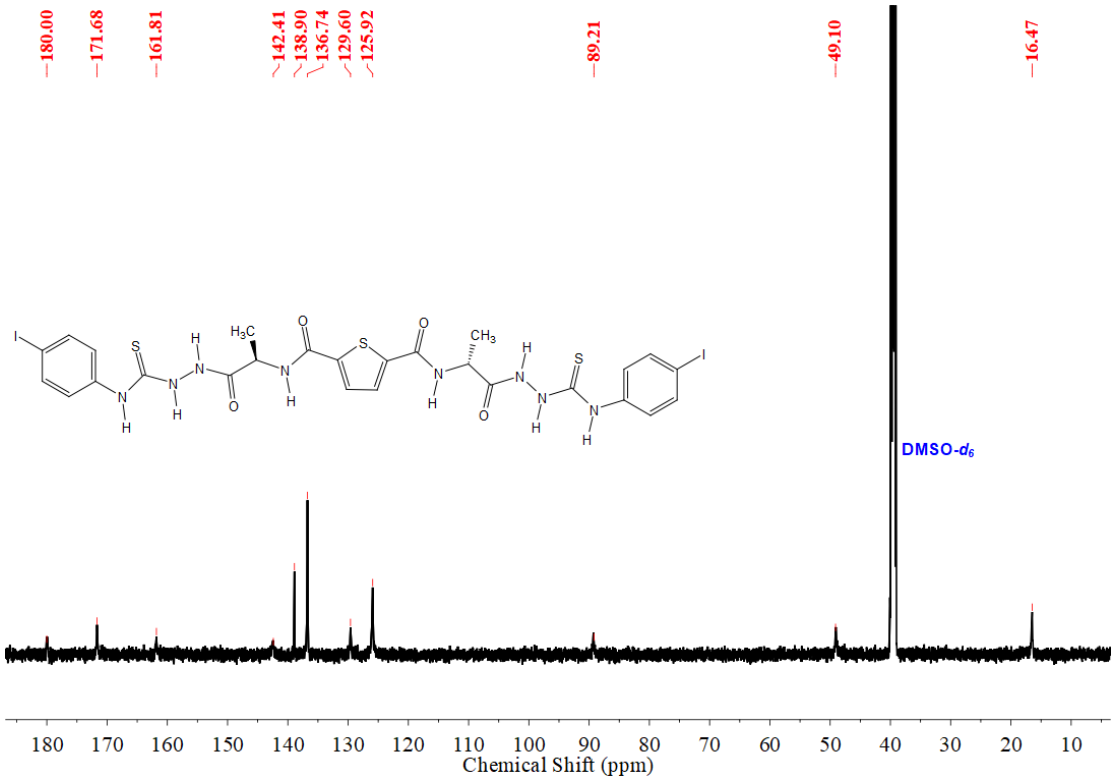

Figure S25. ^{13}C{^{1}H} NMR (151 MHz, DMSO-d_6) spectrum of isolated product D,D-**TAI**.

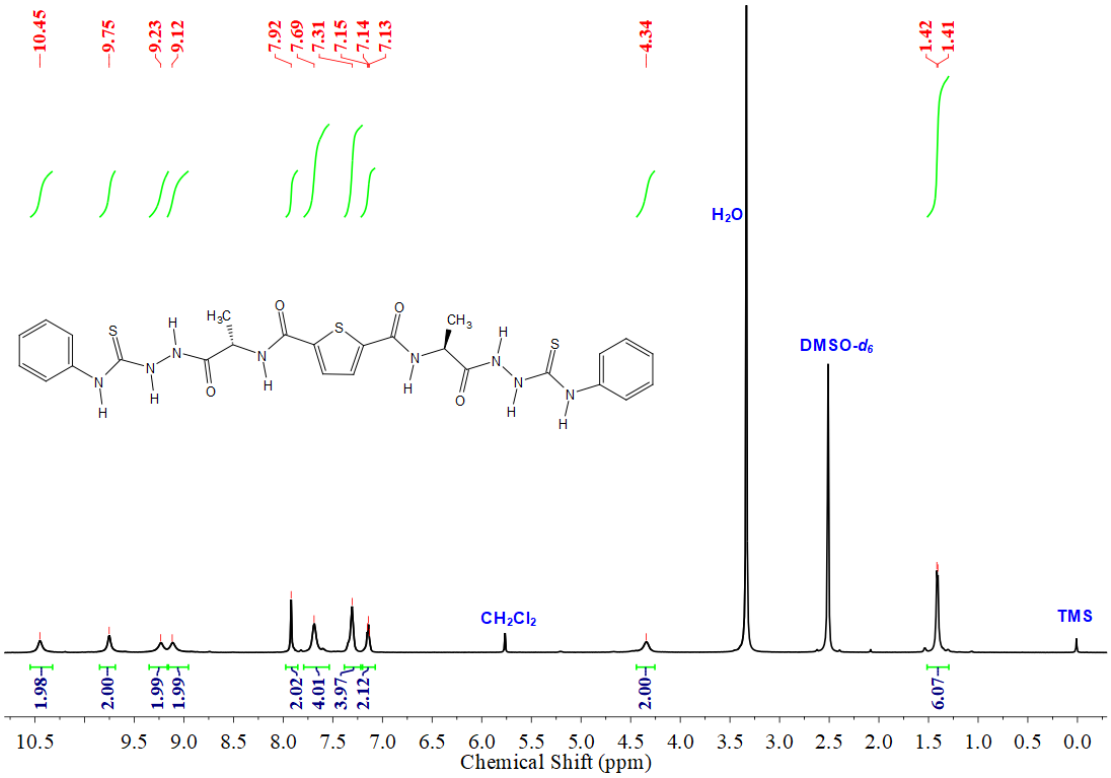

Figure S26. ^{1}H NMR (600 MHz, DMSO-d_6) spectrum of isolated product L,L-**TAH**.

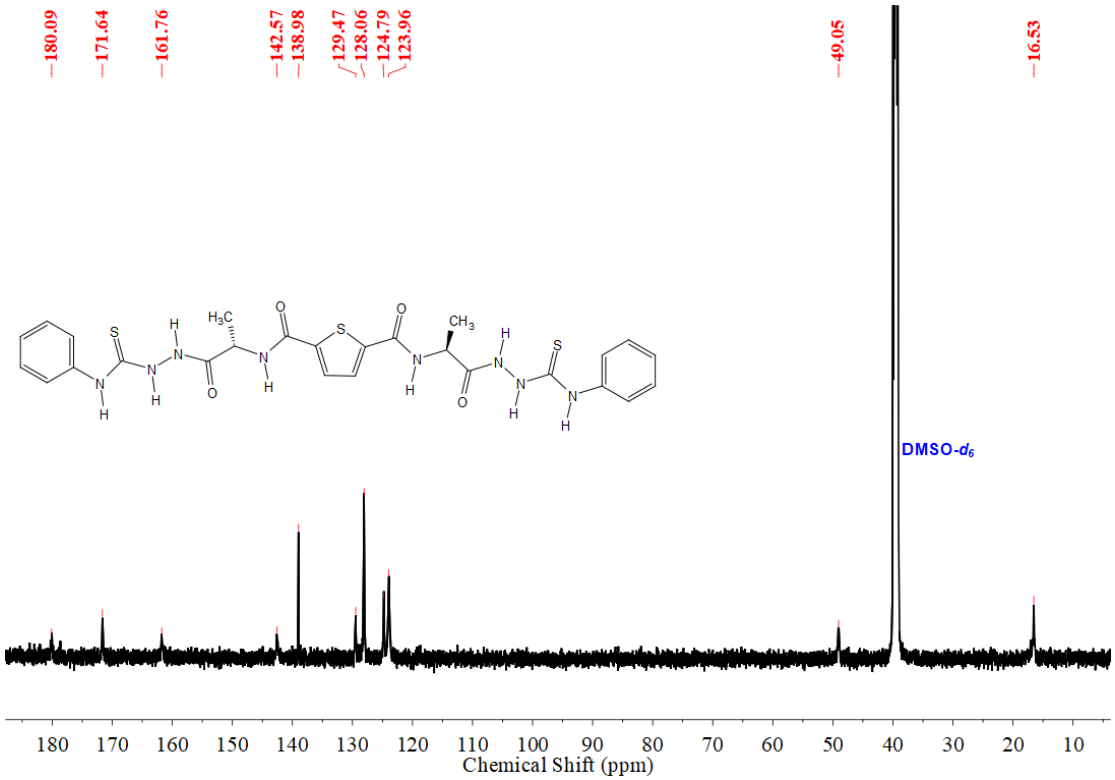

Figure S27. ^{13}C{^{1}H} NMR (151 MHz, DMSO-d_6) spectrum of isolated product L,L-**TAH**.

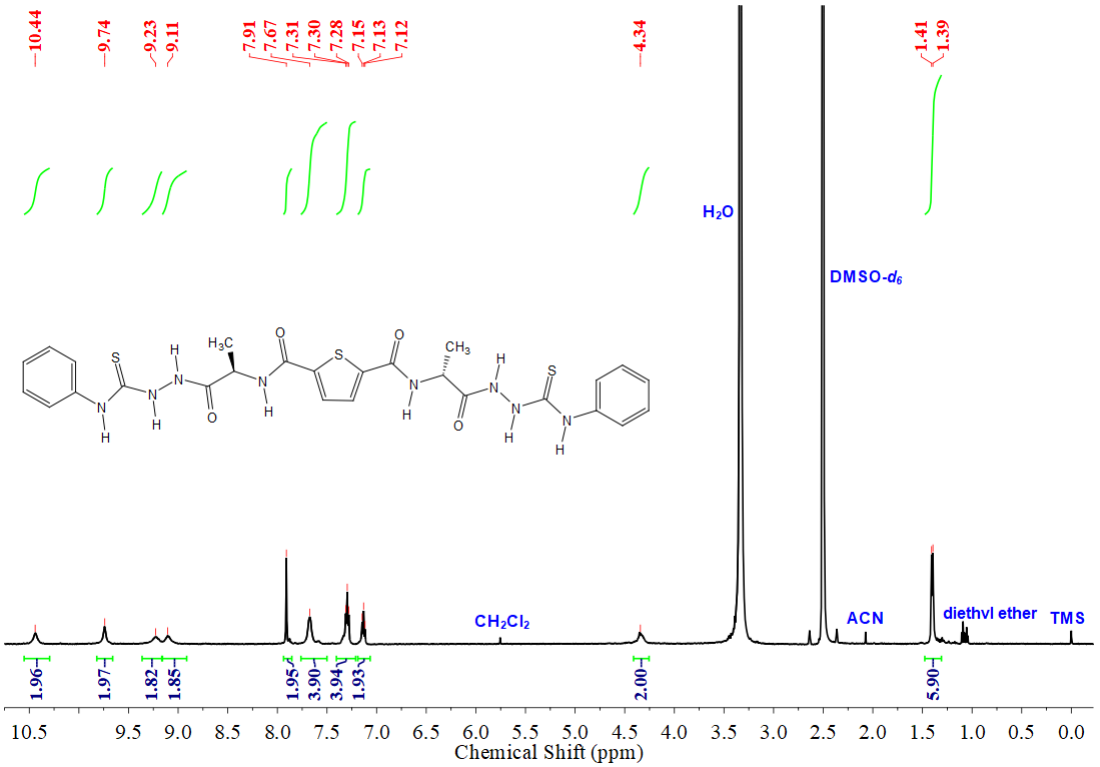

Figure S28. ^{1}H NMR (600 MHz, DMSO-d_6) spectrum of isolated product D,D-**TAH**.

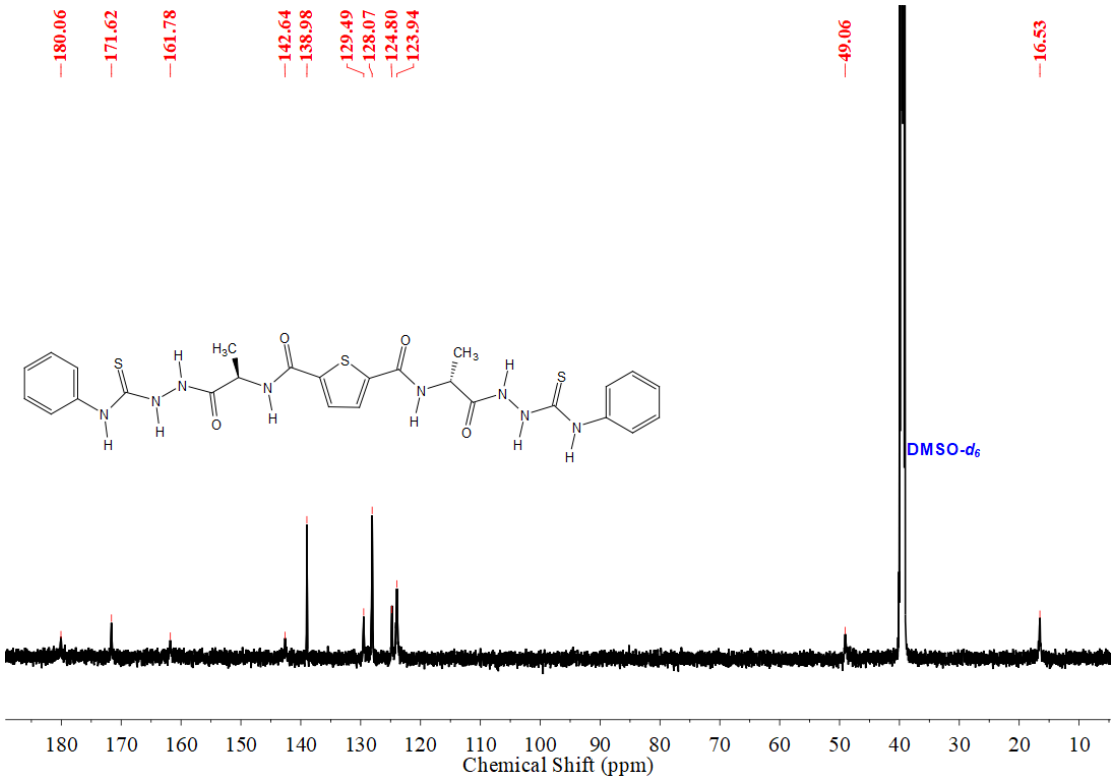

Figure S29. ^{13}C{^{1}H} NMR (151 MHz, DMSO-d_6) spectrum of isolated product D,D-**TAH**.

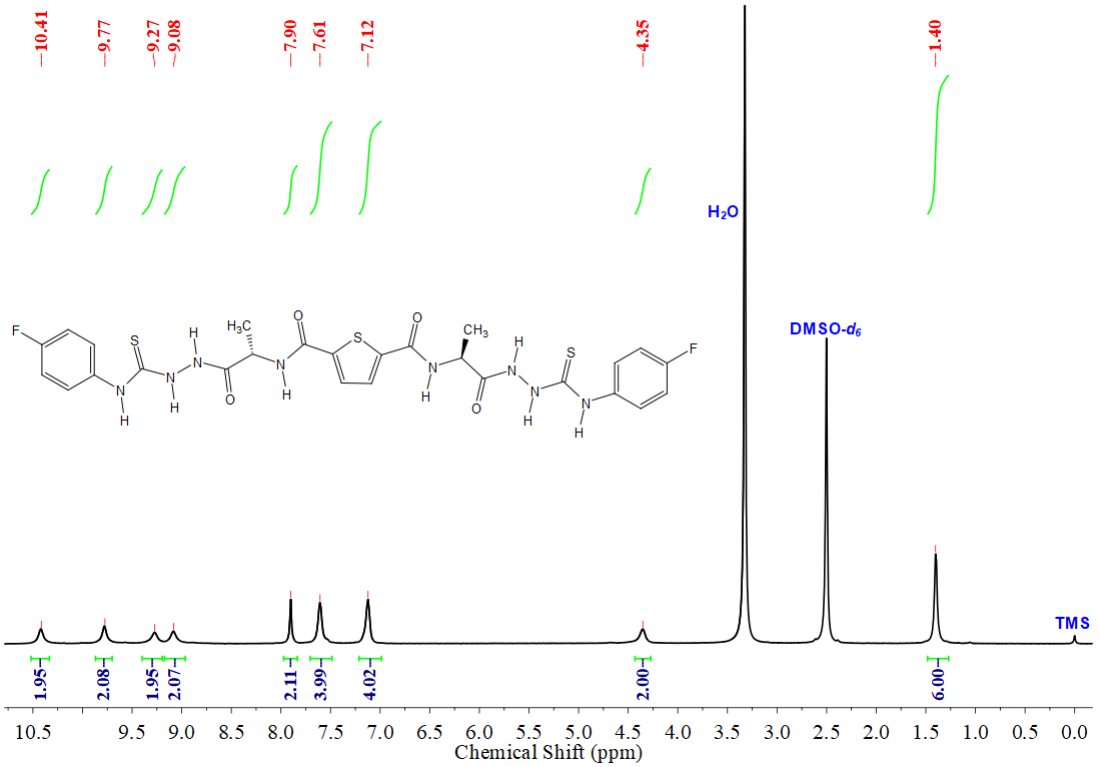

Figure S30. ^{1}H NMR (600 MHz, DMSO-d_6) spectrum of isolated product L,L-**TAF**.

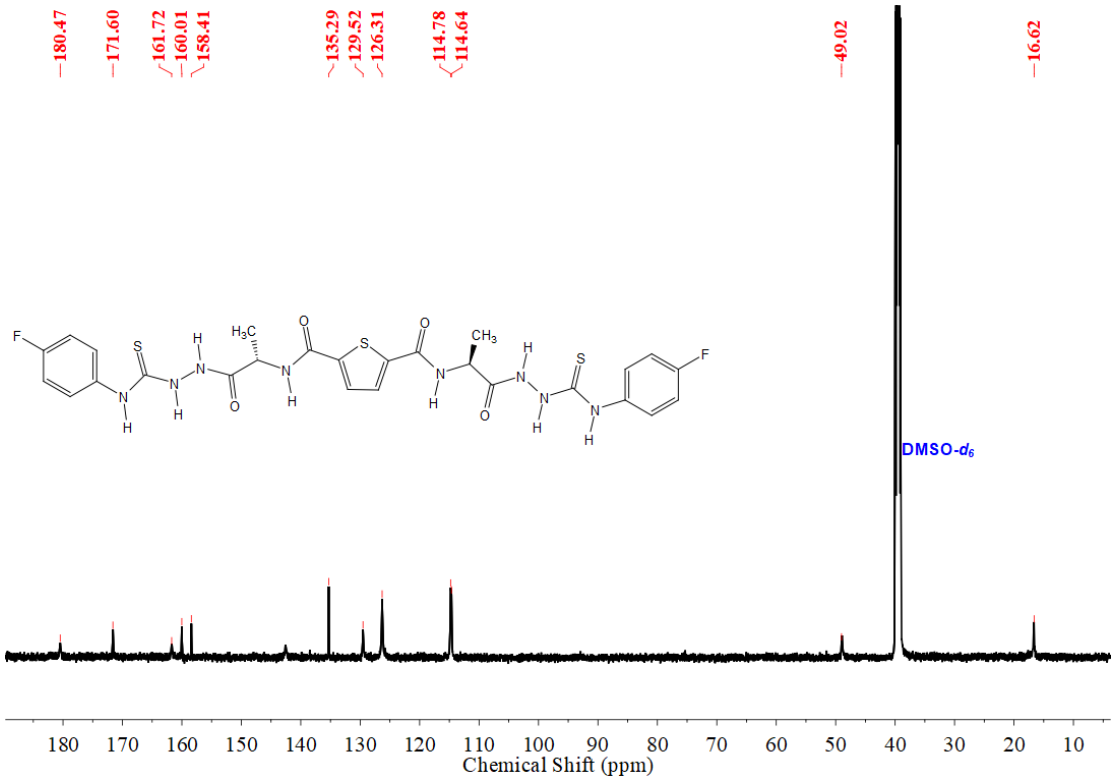

Figure S31. ^{13}C{^{1}H} NMR (151 MHz, DMSO-d_6) spectrum of isolated product L,L-**TAF**.

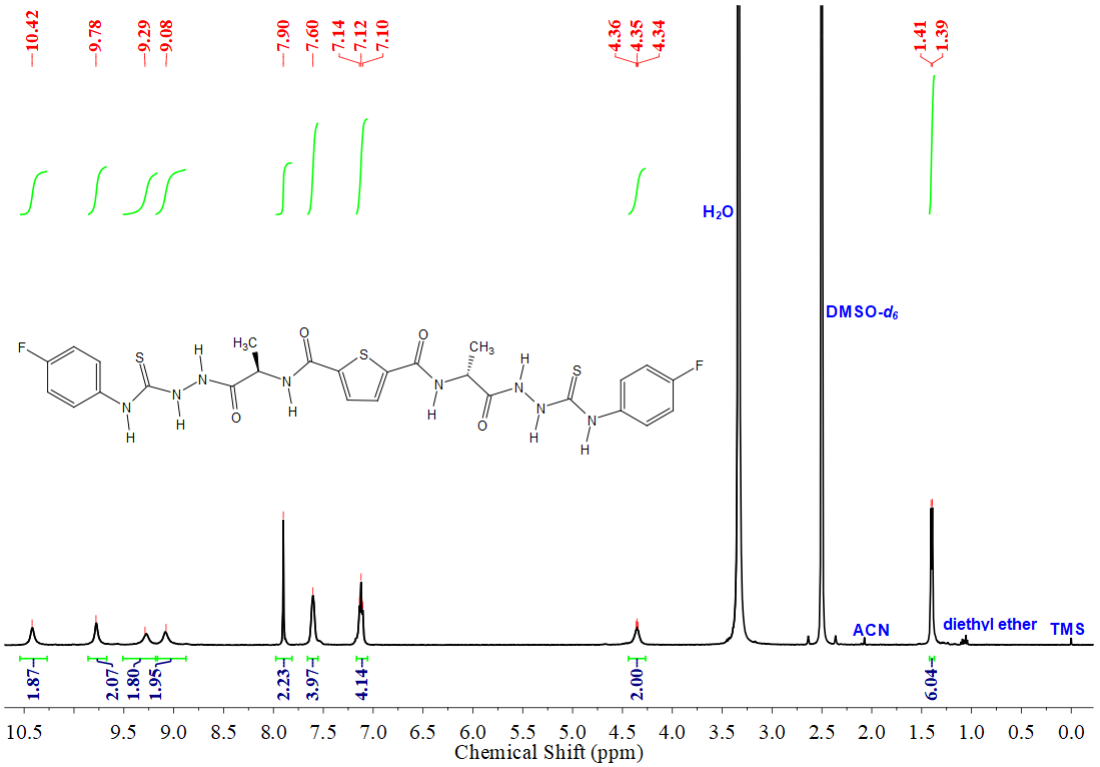

Figure S32. ^{1}H NMR (600 MHz, DMSO-d_6) spectrum of isolated product D,D-**TAF**.

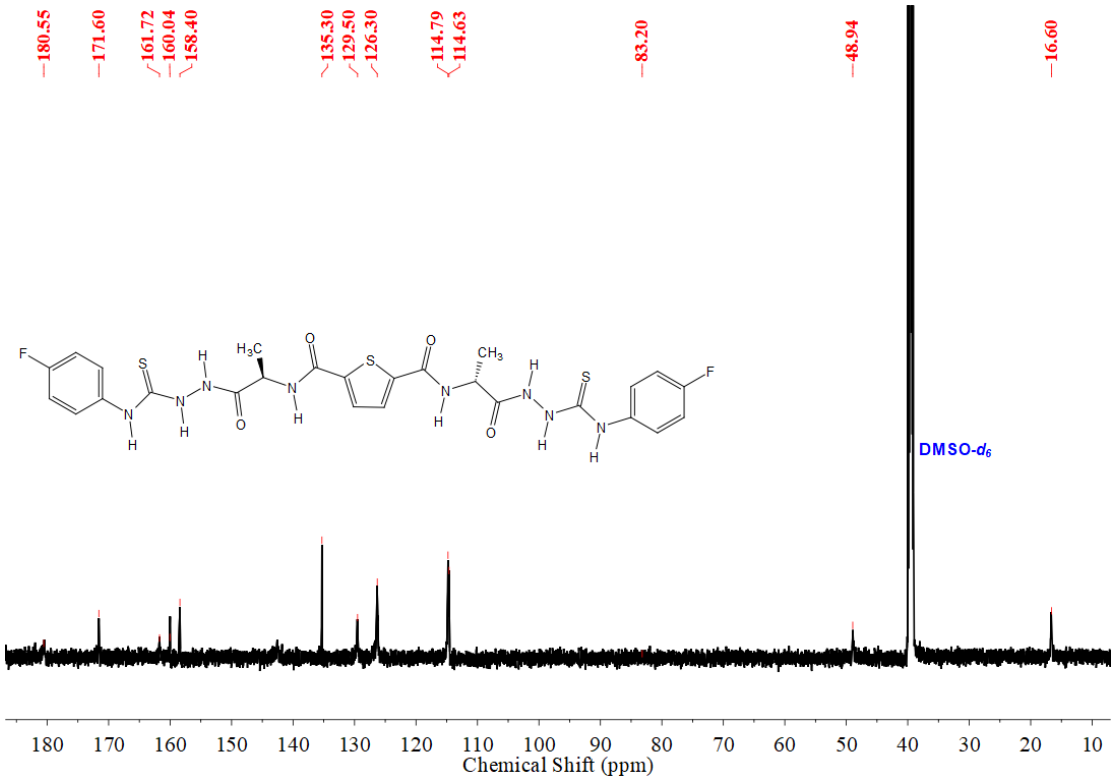

Figure S33. ^{13}C{^{1}H} NMR (151 MHz, DMSO-d_6) spectrum of isolated product D,D-**TAF**.

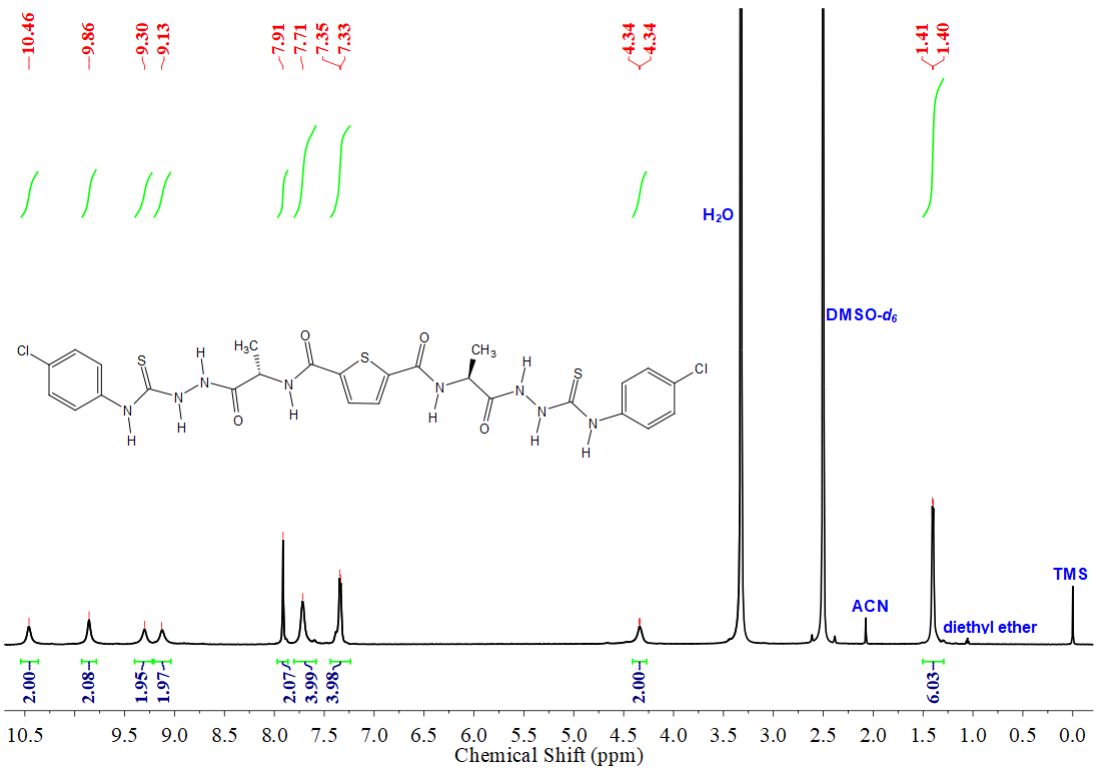

Figure S34. ^{1}H NMR (600 MHz, DMSO-d_6) spectrum of isolated product L,L-**TACl**.

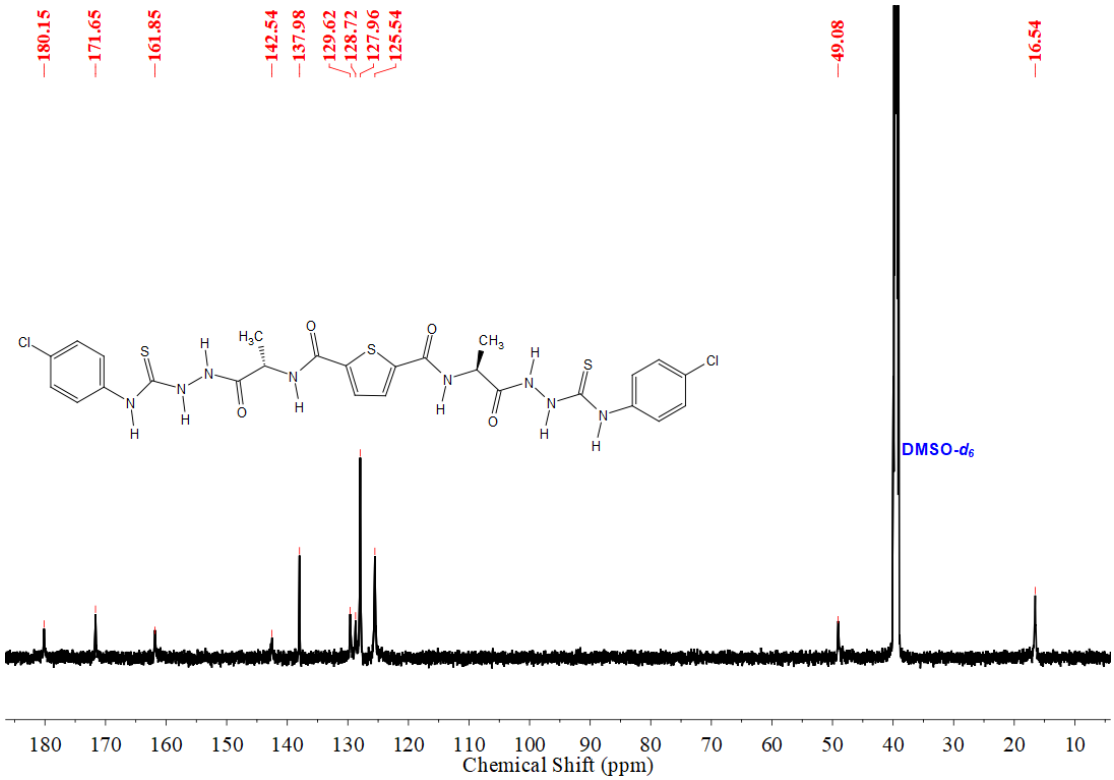

Figure S35. ^{13}C{^{1}H} NMR (151 MHz, DMSO-d_6) spectrum of isolated product L,L-**TACl**.

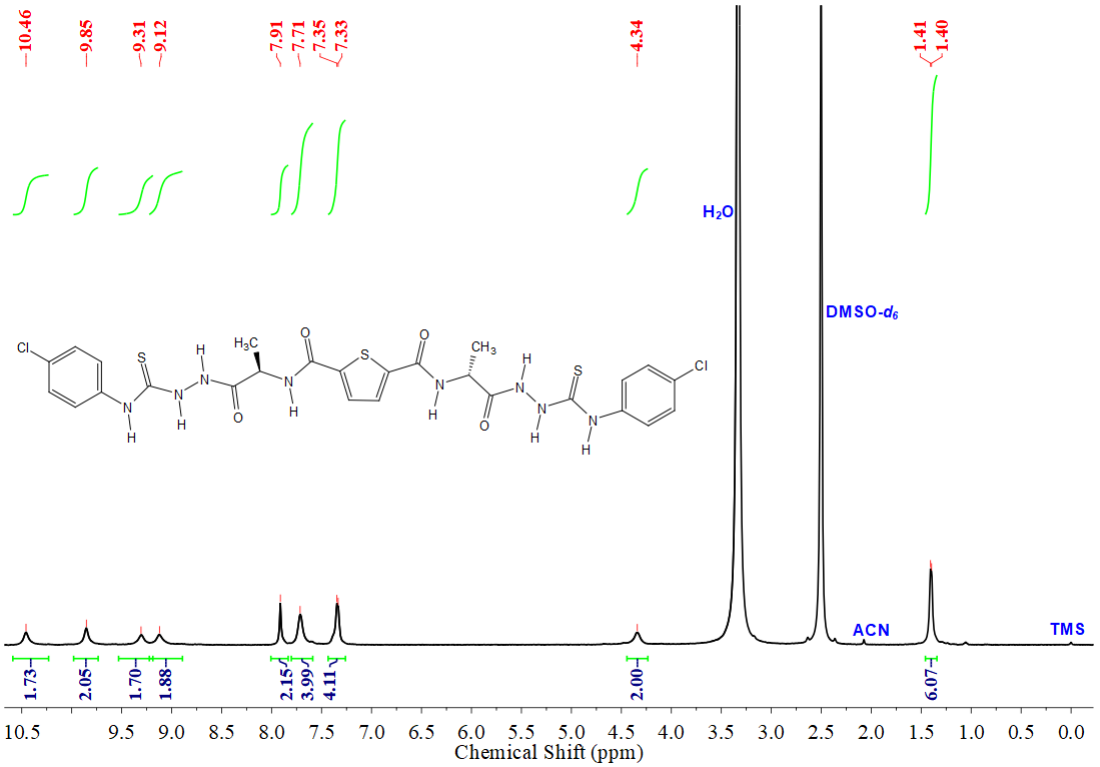

Figure S36. ^{1}H NMR (600 MHz, DMSO-d_6) spectrum of isolated product D,D-**TACl**.

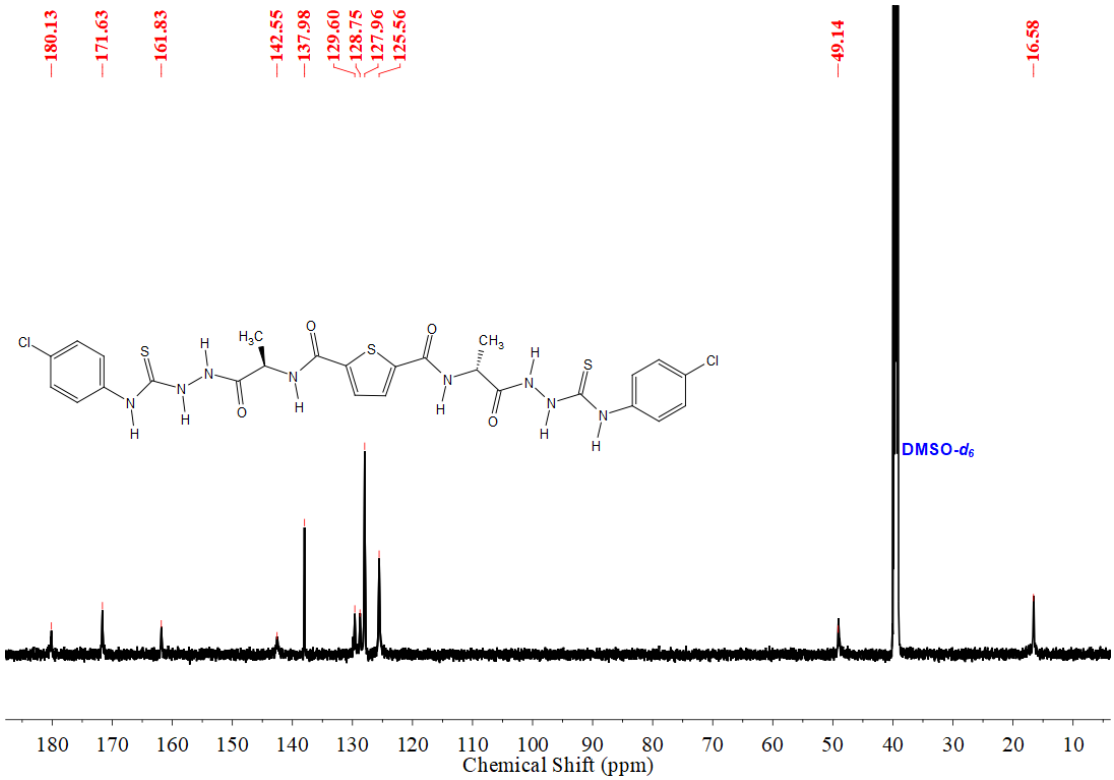

Figure S37. ^{13}C{^{1}H} NMR (151 MHz, DMSO-d_6) spectrum of isolated product D,D-**TACl**.

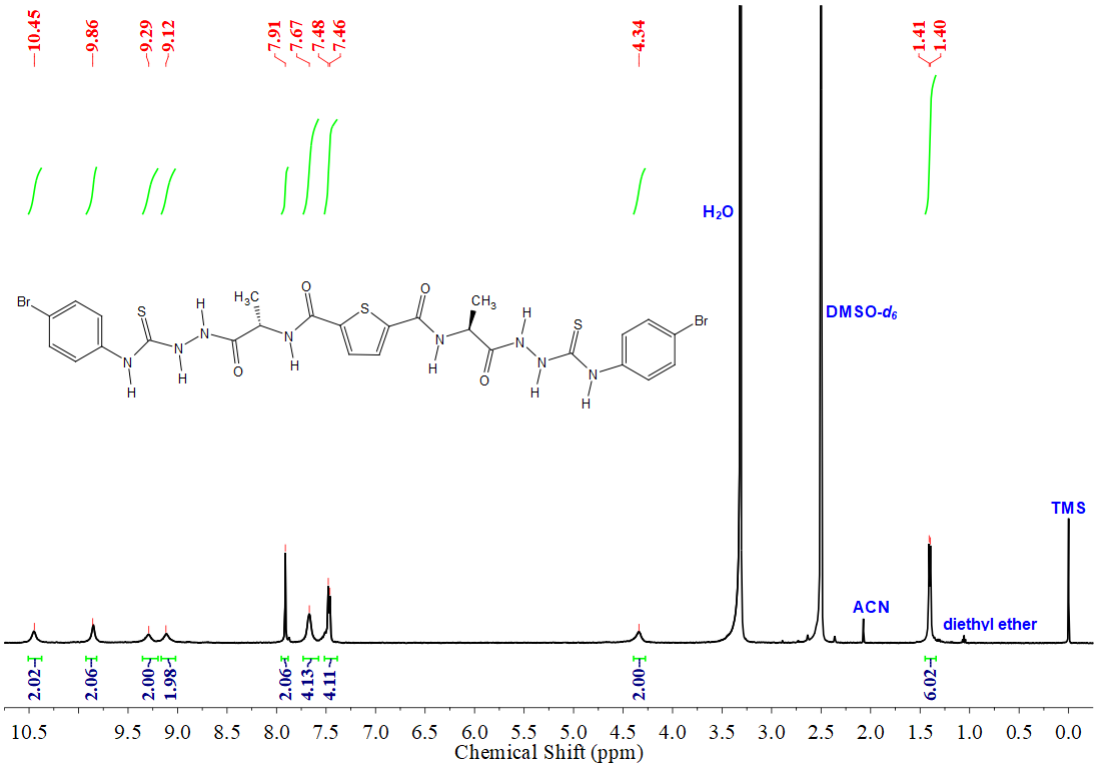

Figure S38. ^{1}H NMR (600 MHz, DMSO-d_6) spectrum of isolated product L,L-**TABr**.

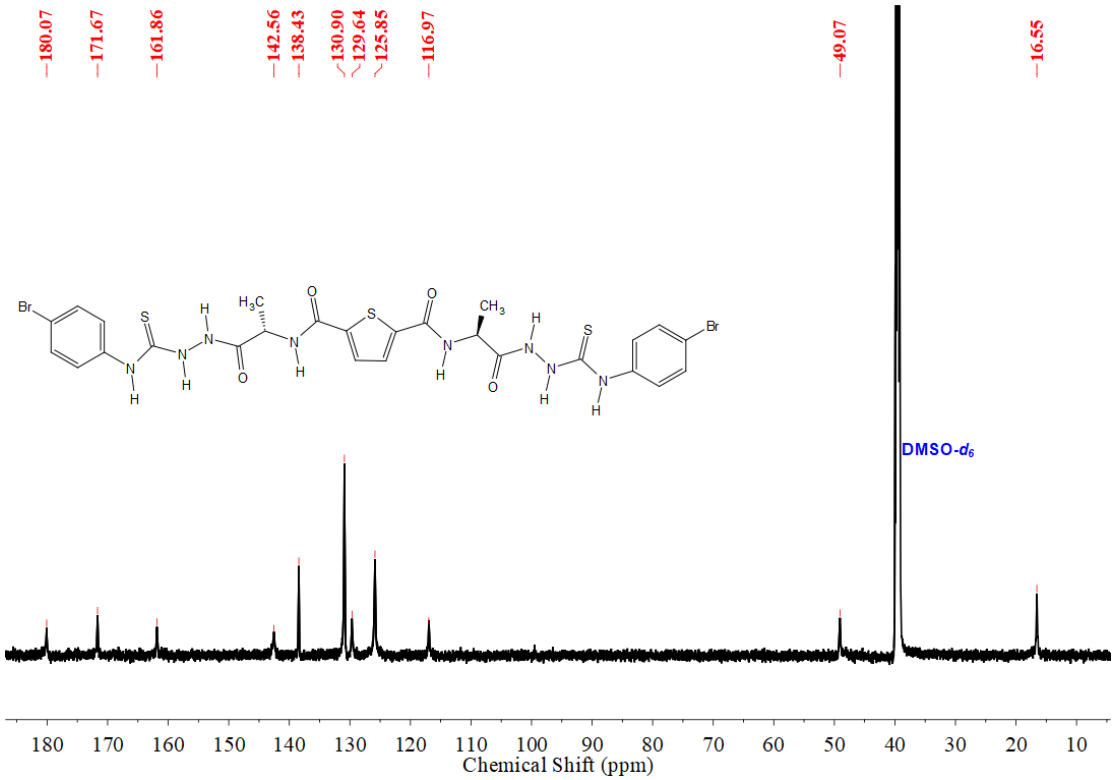

Figure S39. ^{13}C{^{1}H} NMR (151 MHz, DMSO-d_6) spectrum of isolated product L,L-**TABr**.

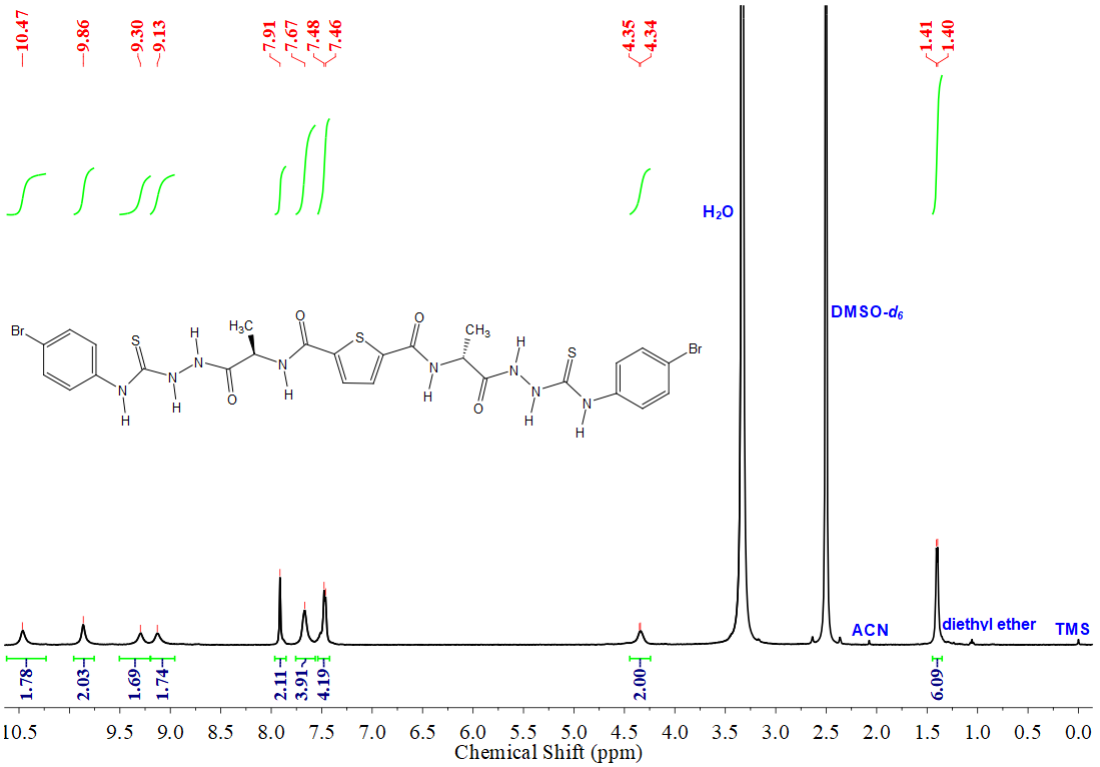

Figure S40. ^{1}H NMR (600 MHz, DMSO-d_6) spectrum of isolated product D,D-**TABr**.

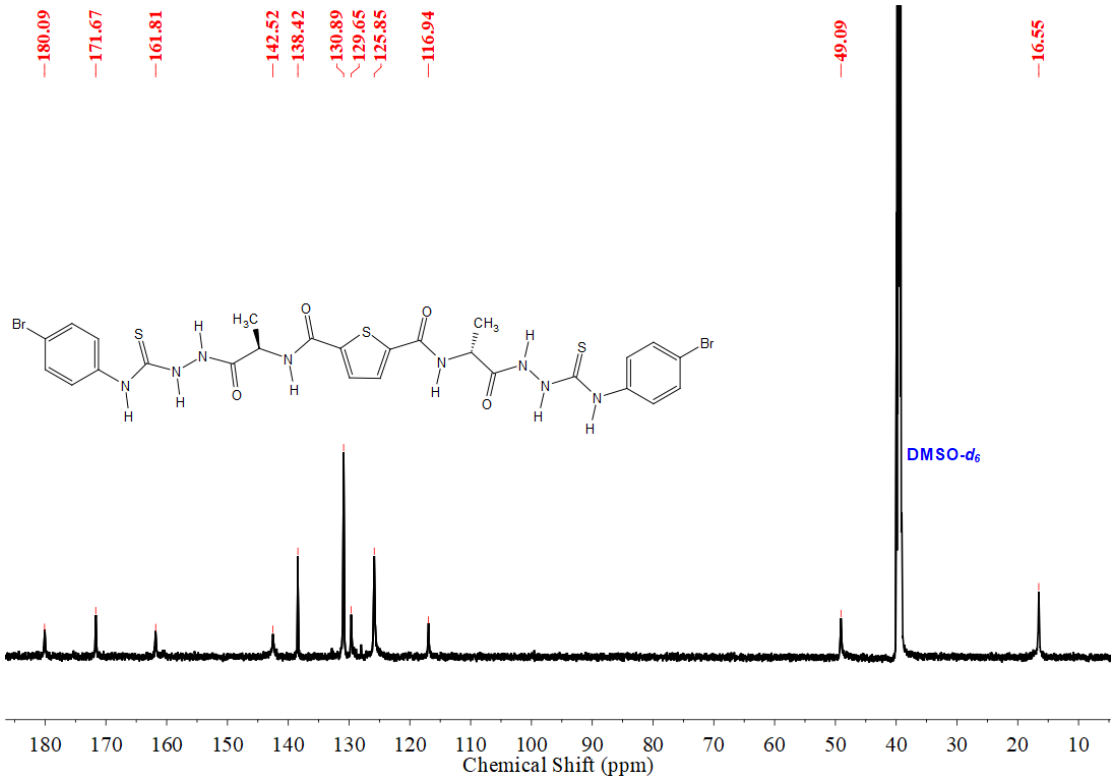

Figure S41. ^{13}C{^{1}H} NMR (151 MHz, DMSO-d_6) spectrum of isolated product D,D-**TABr**.

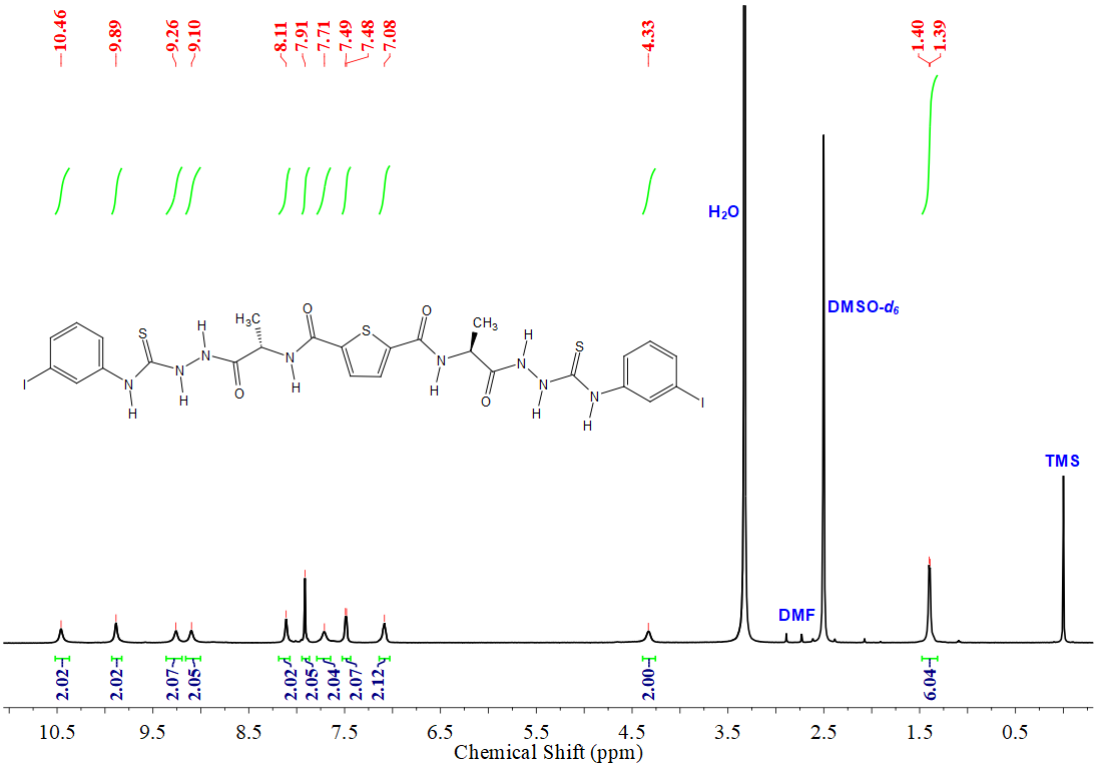

Figure S42. ^{1}H NMR (600 MHz, DMSO-d_6) spectrum of isolated product L,L-*m***TAI**.

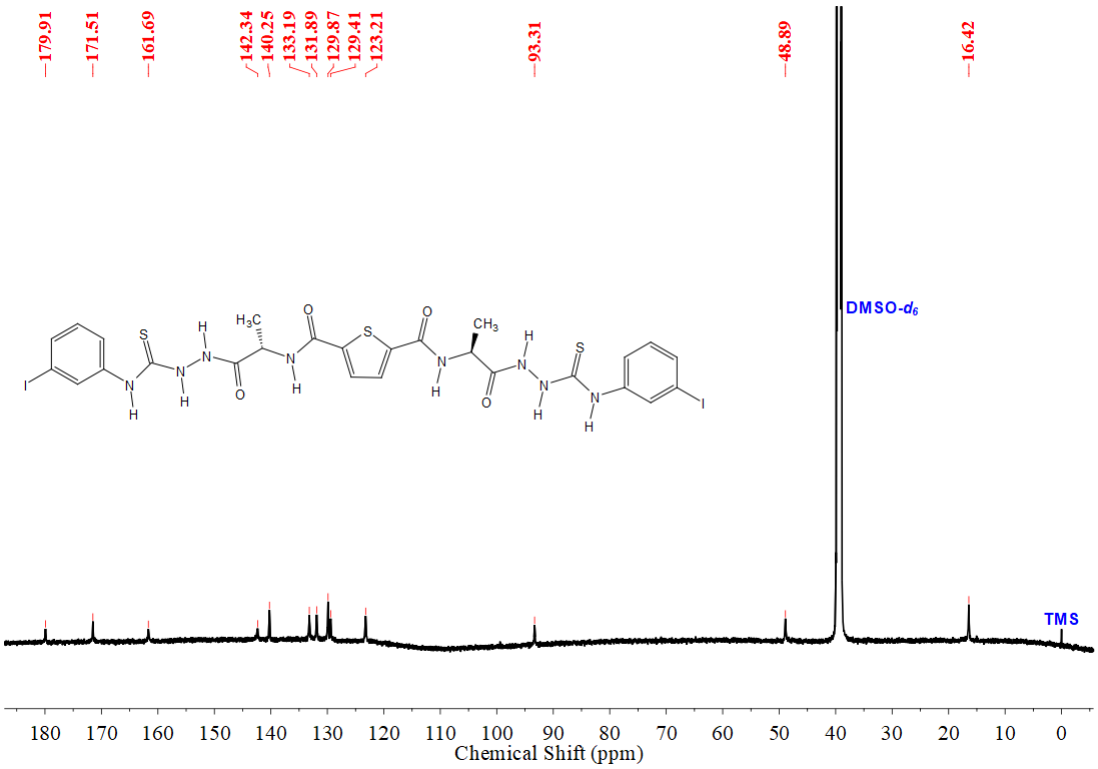

Figure S43. ^{13}C{^{1}H} NMR (151 MHz, DMSO-d_6) spectrum of isolated product L,L-*m***TAI**.

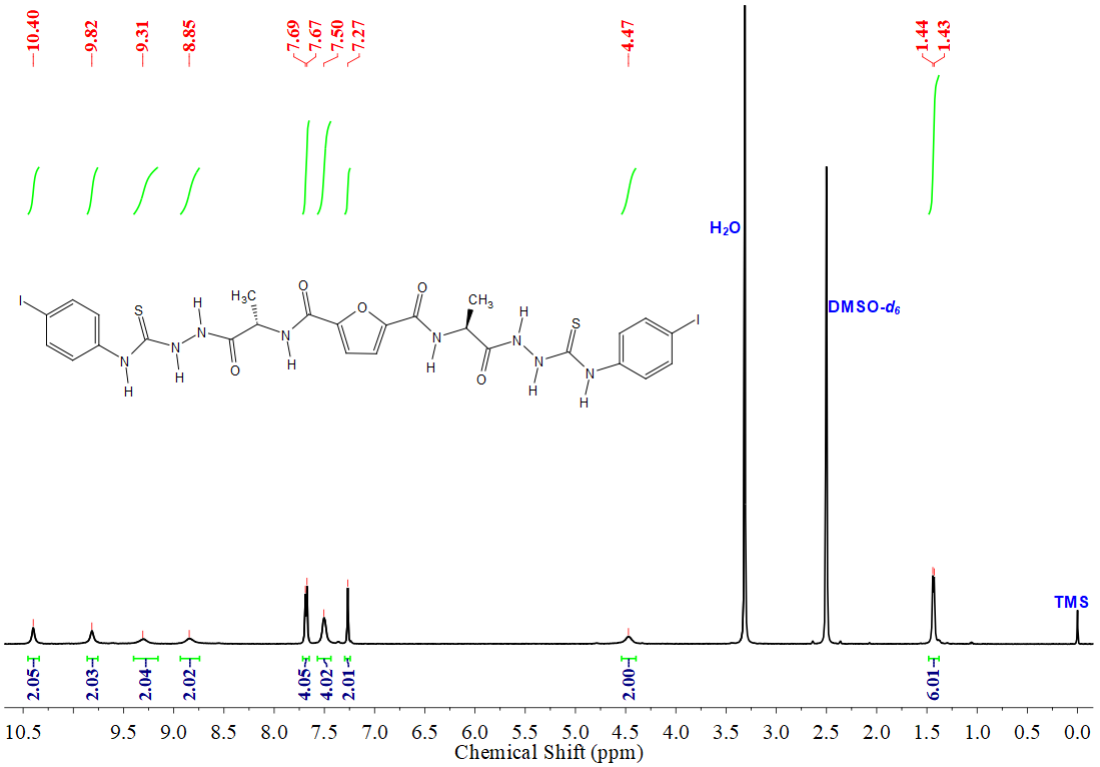

Figure S44. ^{1}H NMR (600 MHz, DMSO-d_6) spectrum of isolated product L,L-**FAI**.

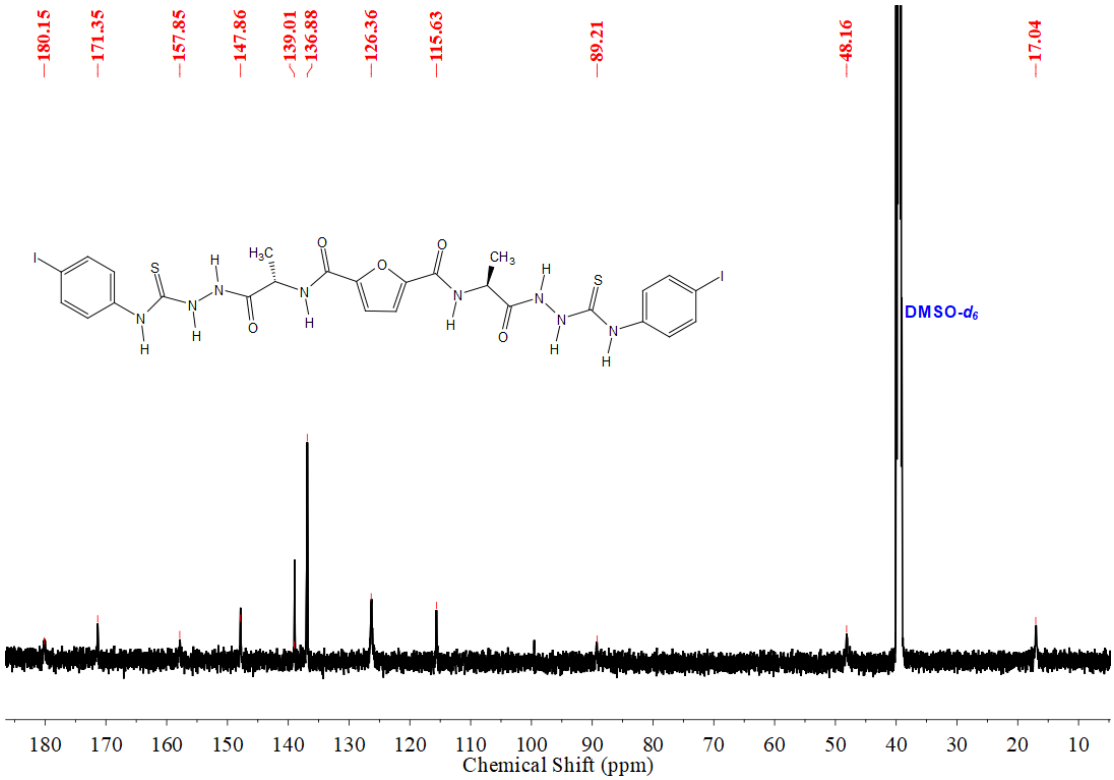

Figure S45. ^{13}C{^{1}H} NMR (151 MHz, DMSO-d_6) spectrum of isolated product L,L-**FAI**.

6. Supplementary references

1. A. L. Spek, *Acta Cryst.*, 2015, C**71**, 9-18.

2. A. E. Reed, L. A. Curtiss and F. Weinhold, *Chem. Rev.*, 1988, **88**, 899-926.

3. T. Lu and F. Chen, *J. Comput. Chem.*, 2012, **33**, 580-592.

4. N. Mohan and C. H. Suresh, *J. Phys. Chem. A*, 2014, **118**, 1697-1705.

5. P. P. Zhou and W. Y. Qiu, *J. Phys. Chem. A*, 2009, **113**, 10306-10320.